Technische Universität München
Fakultät für Physik
Ludwig-Maximilians-Universität München
Fakultät für Physik

Master thesis in the program
Theoretical and Mathematical Physics

Anomalous Quantum Oscillations in Multi-Band Metals with Electronic Interactions

Przemysław Bieniek

Abstract

Quantum oscillations are a powerful tool for determining electronic properties of metals. Due to the relation between the quantum oscillation frequency and the area enclosed by the Fermi surface, measuring quantum oscillations provides insight into the Fermi surface geometry. In recent years, oscillation frequencies equal to combinations of the standard frequencies have been observed in thermodynamics and conductivity in systems with multiple Fermi pockets. Questioning the canonical theory, a theory of interband impurity scattering was proposed to explain the appearance of the difference frequency in conductivity measurements and its temperature stability. In this thesis, I investigate the impact of interband electronic interactions on the quantum oscillation spectrum. I show that the interactions lead to the appearance of a low-temperature difference frequency in thermodynamics and conductivity. The combination of impurity and interaction effects produces a non-Lifshitz-Kosevich temperature dependence of the difference frequency amplitude. The derived theoretical model is related to previous experimental results. A fit to temperature dependence measured in CoSi demonstrates agreement between the model and the data. The here proposed theory enlarges the understanding of quantum oscillations in the presence of interactions.

Acknowledgements

I would like to thank Johannes Knolle for his invaluable guidance in working on this thesis, as well as Valentin Leeb for his advice and a very thorough review of my work.

I would also like to thank Avedis Neehus, Léo Mangeolle and Piotr Kulik for helpful discussions. Additionally, I would like to thank Luis Walther for proofreading this thesis.

Finally, I would like to thank my parents, as their unending support made completing my studies possible.

Contents

Chapter 1

Introduction

The study of conductive materials has been an active field of physics since the development of the electromagnetic theory. Proper understanding of the problem eluded physicists until the advent of the atomic theory – only then conduction could be explained as the motion of electrons in a background of ionized atoms. An early example of a successful theory is the Drude model [1], where the electrons are imagined as classically moving particles that scatter off of positively charged atomic cores.

With the advent of the quantum theory, it became clear that to obtain a full understanding of the behavior of electrons in a metal, a treatment of many-body quantum systems is required. At first glance, the problem seems impossibly complex – even solving the Schrödinger equation in the case of a single particle is no easy task, and in a macroscopic metal there are roughly 10^{23} electrons. Thankfully, there is no need to find the behavior of each individual electron in metals. What is usually of interest are the macroscopic properties arising due to the collective motion of the constituents of the system. Therefore, methods of statistical physics can be used to drastically simplify the problem.

The simplest quantum model of electrons in a metal is a gas of free fermions [2]. There, the particles move freely without interacting with each other. However, they influence each other due to the Pauli exclusion principle – no two fermions can occupy the same quantum state. Because of that, the ground state is not just a group up of electrons in the lowest-energy single-particle state. Instead, the electrons fill states in a bounded region in momentum space, termed the Fermi sea. The boundary of this region is called the Fermi surface. The excitations above the ground state are states where electrons close to the Fermi surface leave the Fermi sea, leaving behind a hole.

Although the free fermion model is extremely simplified, it is surpris-

ingly effective at describing the behaviour of electrons in real metals (where interactions between electrons and between electrons and atomic cores are expected to play a role). This is explained by the concept of a Fermi liquid [3, 4]. When one imagines adiabatically "turning on" the interactions, the ground state and the first excited states of the free gas are expected to be smoothly transformed into the ground state and the first excited states of the Hamiltonian with interactions. Therefore, the structure of states close to the Fermi surface is preserved in the presence of interactions and only constants like the electron mass are renormalized to new values. Provided the interactions are sufficiently weak, the insights from the free Fermi gas can still be used in the case of interacting electrons.

The geometry of a metal's Fermi surface determines its low-energy behaviour. Therefore, tools to measure it are of particular interest. One such method is measuring oscillations of thermodynamical and transport quantities in a metal as a function of the magnetic field, which allows to access the geometry of the Fermi surface directly! When a metal is placed in a magnetic field, and then e.g. conductivity of the material is measured as a function of the magnetic field, one finds that it oscillates as $\sigma \sim \cos\left(2\pi \frac{F}{B}\right)$. The frequency of oscillations turns out to be related to the area inside of the Fermi surface $\mathcal{A}$ (in two dimension) or the area of the extremal cross-section of the Fermi surface perpendicular to the magnetic field (in three dimensions) as $\mathcal{A} = eF$.

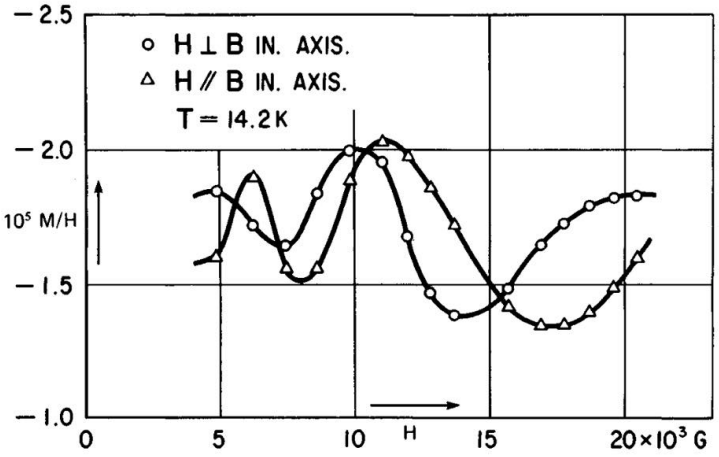

Figure 1.1: First evidence of quantum oscillations of magnetic susceptibility, observed by de Haas and van Alphen in bismuth [5].

Oscillations in thermodynamic quantities were first discovered in 1930 by de Haas and van Alphen [5], and in conductivity in the same year by Shub-

nikov and de Haas [6]. An insightful semiclassical explaination was provided in 1952 by Onsager [7], establishing the connection between oscillation frequencies and the area inside of the Fermi surface. A full quantum description was devised by Lifshitz and Kosevich in 1956 [8]. An upshoot was the temperature dependence of the quantum oscillation amplitude. In the case of a two dimensional electron gas, it follows

$$R_{LK}(\chi) = \frac{\chi}{\sinh \chi} \tag{1.1}$$

with $\chi = \frac{2\pi^2 mT}{eB}$, where T is the temperature, m the effective mass, e the electron charge and B the external magnetic field. This temperature damping is another reason why measuring magnetic oscillations is a powerful experimental tool – it can be used to determine the effective particle mass m in a metal.

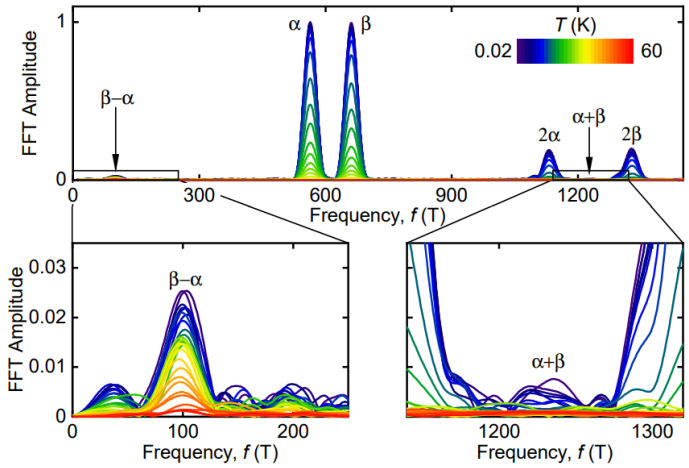

Figure 1.2: The Fourier transform of longitudinal conductivity as a function of the magnetic field measured in CoSi [9]. Noticeable peaks are at fundamental frequencies α, β, second harmonics 2α, 2β and sum and difference frequencies $\beta \pm \alpha$. The curves of different colors denote measurements at different temperatures – note the surprising temperature stability of the difference frequency peak!

The standard theory of quantum oscillations has been enormously successful, finding confirmation in countless experiments and being widely used to investigate electronic properties of metals. In recent years, deviations from the standard theory have been found in a number of materials, like the appearance of quantum oscillations in bulk insulators [10, 11] and heterostructures [12, 13]. Of particular interest to this work is the discovery

of combination frequencies. In materials with multiple distinct Fermi pockets (enclosing areas $\mathcal{A}_1$, $\mathcal{A}_2$), in addition to frequencies proportional to $\mathcal{A}_1$, $\mathcal{A}_2$ individually, frequencies proportional to $k_1\mathcal{A}_1 \pm k_2\mathcal{A}_2$ with integer k_1, k_2 have been observed in thermodynamics [14–17] and conductivity [9]. The difference frequency proportional to $\mathcal{A}_1 - \mathcal{A}_2$ in conductivity is especially interesting, as it has been shown to survive to surprisingly high temperatures [9].

A model explaining the appearance of the combination frequencies in multi-band materials has recently been proposed by Leeb and Knolle [18]. There, electrons from different bands can scatter on impurities to change their band index. This causes the self-energy associated with a single band to oscillate as a function of $\frac{1}{B}$ with frequencies proportional to areas of both Fermi pockets, which in turn produces the combination frequencies in observables. The model predicts the appearance of the sum and difference frequency in conductivity and only the sum frequency in thermodynamical quantities. Moreover, the difference frequency term in conductivity depends on temperature through the LK factor Eq. (1.1), but with χ proportional to the difference of effective masses of the two bands $m_1 - m_2$. This explains the remarkable temperature stability of the difference frequency – when $m_1 \approx m_2$, $R_{LK}(\chi)$ decays very slowly.

The theory of Leeb and Knolle is promising as a model of combination frequency QOs, but does not explain all of their experimentally observed features. In a resistivity measurement in CoSi [9], the difference frequency amplitude indeed survives to a high temperature ~ 70 K, but additionally it slightly drops in longitudinal conductivity and increases in transversal conductivity at low temperatures ~ 1 K. Additionally, it does not lead to the appearance of the difference frequency in thermodynamics, which has been observed in many other materials [14–16]. This suggests the existence of an additional mechanism, which could produce a difference frequency in thermodynamics, and influence the low-temperature behavior of the amplitude in conductivity.

Besides the scattering of electrons at impurities, it is natural to consider the impact of interactions between electrons on the quantum oscillation spectrum. In the single-band case, they have been shown to only change the amplitude due to spin splitting and introduce a constant shift to the chemical potential [19, 20]. Results for layered metals show that interactions can lead to the appearance of the difference frequency in thermodynamical quantities [21].

In this work, I consider a multi-band model with electronic interactions. I show that allowing electrons from different bands to interact introduces new terms to the real part of the self energy which are temperature damped. This

leads to new difference frequency terms in conductivity and thermodynamics, which depend on temperature through a factor of R_{LK}^2. The resulting temperature dependence of the amplitude in conductivity qualitatively agrees with the one observed in CoSi.

Outline of the work

The thesis is structured as follows. In chapter 2, I lay out the standard theory of quantum oscillations in metals. I begin in section 2.1 with their semiclassical treatment and a few qualitative remarks. In section 2.2, I describe the behavior of a system of fermionic particles in a constant magnetic field. In sections 2.3 and 2.4, I use the results of the previous section to derive the oscillations of thermodynamic quantities and conductivity as a function of the magnetic field. Chapter 3 is dedicated to deriving anomalous quantum oscillations emerging in multi-band systems due to interband impurity scattering and interactions. In section 3.1, I derive the Feynman rules for general impurities and interactions in a system of fermions in a magnetic field. In section 3.2, I compute the lowest-order self-energy contributions using the derived rules. In section 3.3, I generalize the previously considered system to the case of multiple bands and introduce interactions between fermions in different bands. In section 3.4, I show that in a system described in previous sections, there appear new quantum oscillation frequencies with new types of temperature dependence. Finally in section 3.5, I discuss the experimental consequences of my findings.

Chapter 2

Quantum oscillations in conventional metals

2.1 Qualitative treatment

The appearance of oscillations of thermodynamic and transport quantities as a function of the external magnetic field can be seen already on the level of semiclassical analysis. This approach was first developed by Onsager [7], here I recount the main results. I start from the equation of motion of electrons (neglecting Berry phase effects)

$$\dot{\boldsymbol{k}} = -e\boldsymbol{v} \times \boldsymbol{B}, \tag{2.1}$$

which relates the time derivative of the momentum $\boldsymbol{k}$ to the Lorentz force, where $\boldsymbol{v} = \boldsymbol{\nabla}_{\boldsymbol{k}}\varepsilon_{\boldsymbol{k}}$ is the velocity and $\mathbf{B}$ is the external magnetic field. The equation can be integrated with respect to time to obtain

$$\boldsymbol{k} - \boldsymbol{k}_0 = -e(\boldsymbol{r} - \boldsymbol{r}_0) \times \boldsymbol{B}. \tag{2.2}$$

This result means that in the plane perpendicular to $\boldsymbol{B}$ the trajectory of electrons in real space has the same shape as their trajectory in momentum space, only rotated and rescaled by a factor eB. To introduce quantum effects, an additional constraint of the motion of the electrons has to be introduced – the Bohr quantization rule

$$\int \boldsymbol{p} \cdot d\boldsymbol{r} = 2\pi(n + \gamma), \tag{2.3}$$

where $\boldsymbol{p} = \boldsymbol{k} - e\boldsymbol{A}$ is the conjugate momentum to position $\boldsymbol{r}$ and γ is a constant dependant on the form of the dispersion. The integral can be expressed as

$$\int \boldsymbol{p} \cdot d\boldsymbol{r} = \frac{S}{eB}, \tag{2.4}$$

with S being the area inside of the trajectory electrons take in momentum space. Therefore, relation Eq. (2.3) constrains the electrons to trajectories such that the area enclosed by them is quantized in units of $2\pi eB$.

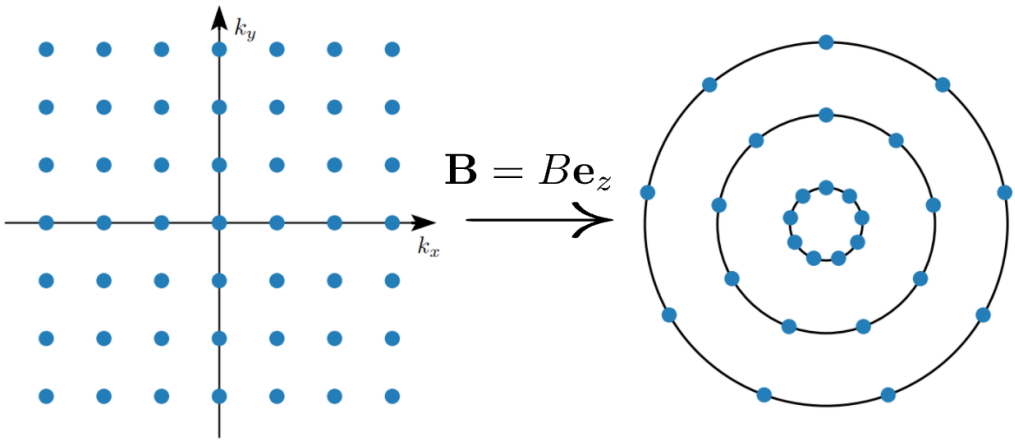

Figure 2.1: The structure of states of a free fermion gas before and after turning on a magnetic field perpendicular to the plane of motion. The free Fermi Hamiltonian is diagonalized by momentum eigenstates, thus the states are located on a lattice in momentum space. With the magnetic field, the lattice collapses onto discrete, degenerate energy levels.

In the full quantum case, the momentum eigenstates usually present in fermionic systems are replaced by discrete energy levels called Landau levels (as I shall show in section 2.2). The levels are evenly spaced in energy and highly degenerate. Using the insight from Eq. (2.3), they can be imagined as circles (or, in the three-dimensional case, cylinders) in momentum space, as depicted in figure 2.1. Of course, this picture is not rigorous, as in the presence of a magnetic field the translation symmetry is broken, making it impossible to diagonalize the Hamiltonian in the momentum basis. However, it is useful to get an intuitive understanding of the problem.

At this point, the appearance of magnetic oscillations of the density of states ρ can be explained. As the magnitude of the magnetic field increases, so does the separation between energy levels and their degeneracy, as depicted in figure 2.2. There will be values of B, for which one of the energy levels is close to the Fermi level, resulting in a high density of states. For other values of B, the density of states will be low. As the magnetic field grows, the energy levels will periodically cross the Fermi energy, resulting in oscillatory behaviour of ρ. The period of these oscillations can be determined from the Bohr quantization rule Eq. (2.3): it will be the difference between two values

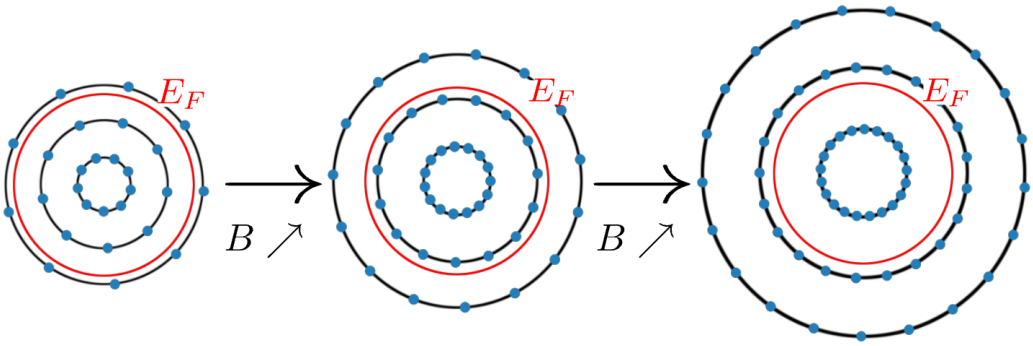

Figure 2.2: The energy levels in a free fermion system with a magnetic field for growing magnitudes of the magnetic field, and a red circle representing the Fermi energy. When the magnetic field increases, the energy levels periodically fall out of the Fermi surface.

of $\frac{1}{B}$, for which one of the energy levels crosses the Fermi surface

$$\frac{1}{B_n} - \frac{1}{B_{n-1}} = \frac{2\pi e}{S}. \tag{2.5}$$

Therefore, the density of states has an oscillatory part behaving like

$$\rho_{osc}(E_F) \sim \cos\left(\frac{S}{eB}\right), \tag{2.6}$$

where S is the area enclosed within the Fermi surface! It is an important result, as it means that by measuring magnetic oscillations (for example in magnetization or conductivity), one can learn about the geometry of the Fermi surface. It becomes more powerful in three dimensions, where S is the area of an extremal cross-section of the Fermi surface perpendicular to the magnetic field. Then, one can measure oscillations with the magnetic field in various directions to discover the shape of the three-dimensional Fermi surface.

2.2 Fermions in a constant magnetic field

To understand further features of magnetic oscillations, they have to be described within a microscopic theory [8]. I restrict my considerations to the continuum, finite-volume fermion system with quadratic dispersion. However it should be noted that quantum oscillations can be shown to appear in a wide variety of models with different dispersions and lattice geometries [22].

A 2-dimensional gas of free fermions is described by the Hamiltionian

$$H = \int d^2\boldsymbol{r}\phi^\dagger(\boldsymbol{r}) \left(-\frac{\boldsymbol{\nabla}^2}{2m} - \mu \right) \phi(\boldsymbol{r}), \tag{2.7}$$

where m is the effective electron mass and μ is the chemical potential. Using the minimal coupling scheme, the magnetic field can be included by transforming $\boldsymbol{p} \to \boldsymbol{p} - e\boldsymbol{A}$, where $\boldsymbol{A}$ is the vector potential fulfilling $\boldsymbol{B} = \boldsymbol{\nabla} \times \boldsymbol{A}$. Then, the Hamiltonian takes the form

$$H = \int d^2\boldsymbol{r}\phi^\dagger(\boldsymbol{r}) \left(-\frac{(\boldsymbol{\nabla} + \mathrm{i}e\boldsymbol{A})^2}{2m} - \mu \right) \phi(\boldsymbol{r}). \tag{2.8}$$

The case of interest is that of a constant magnetic field perpendicular to the plane of motion of the electrons, $\boldsymbol{B} = B\boldsymbol{e}_z$. The treatment of this system was first developed by Landau [23]. One choice for the vector potential leading to this magnetic field is $\boldsymbol{A} = -By\boldsymbol{e}_x$. With this vector potential, the Hamiltonian is

$$H = \int d^2\boldsymbol{r}\phi^\dagger(\boldsymbol{r}) \left(-\frac{(\partial_x - \mathrm{i}eBy)^2}{2m} - \frac{\partial_y^2}{2m} - \mu \right) \phi(\boldsymbol{r}). \tag{2.9}$$

To diagonalize it, I first utilize the translation symmetry in the x direction and perform a Fourier transform

$$\phi(\boldsymbol{r}) = \frac{1}{\sqrt{L_x}} \sum_{k_x} \mathrm{e}^{\mathrm{i}k_x x} \phi_{k_x}(y), \tag{2.10}$$

changing the Hamiltonian into

$$H = \int dy \sum_{k_x} \phi_{k_x}^\dagger(y) \left(\frac{(k_x - eBy)^2}{2m} - \frac{\partial_y^2}{2m} - \mu \right) \phi_{k_x}(y). \tag{2.11}$$

Now, one may notice the similarity to the Hamiltonian of the quantum harmonic oscillator - it contains terms quadratic in ∂_y and y. To exploit this feature, I transform the field in the following way:

$$\phi_{k_x}(y) = \sum_{l=0}^{\infty} \psi_l \left(y - \frac{k_x}{eB} \right) \phi_{k_x,l}, \tag{2.12}$$

where ψ_l is the wavefunction of the quantum harmonic oscillator:

$$\psi_l(y) = \frac{1}{\sqrt{2^l l!}} \left(\frac{eB}{\pi} \right)^{\frac{1}{4}} \mathrm{e}^{-\frac{1}{2}eBy^2} H_l\left(\sqrt{eB}y \right), \tag{2.13}$$

with H_l being the l-th Hermite polynomial and $\omega_c = \frac{eB}{m}$ being the cyclotron frequency. Substituting Eq. (2.12) into Eq. (2.9) and carrying out the derivatives and position integrals, the Hamiltonian transforms into

$$H = \sum_{l=0}^{\infty} \sum_{k_x} \varepsilon_l \, \phi^\dagger_{k_x,l} \phi_{k_x,l} \tag{2.14}$$

with the dispersion

$$\varepsilon_l = \omega_c \left(l + \frac{1}{2} \right) - \mu. \tag{2.15}$$

The electrons occupy discrete energy levels l called Landau levels. In a finite-size system with sizes L_x, L_y, each level has a finite, but macroscopically high degeneracy. It can be found by noting, the shift $\frac{k_x}{eB}$ appearing in Eq. (2.12) has to lie within the bounds of the system, that is

$$0 \leq \frac{k_x}{eB} \leq L_y. \tag{2.16}$$

Since $k_x = \frac{2\pi n}{L_x}$, the degeneracy is

$$N_\Phi = \frac{eBL_xL_y}{2\pi} = \frac{\Phi}{\Phi_0} \tag{2.17}$$

and is equal to the amount of elementary magnetic flux quanta $\Phi_0 = \frac{2\pi}{e}$ in the system.

To compute observables – thermodynamic quantities like magnetization and transport quantities like conductivity – I make use of the Green's function formalism. For the Hamiltonian Eq. (2.14), the full Green's function can be immediately read off to be

$$G^0_l(i\omega_n) = \frac{1}{\mathrm{i}\omega_n - \varepsilon_l}, \tag{2.18}$$

where $\omega_n = \frac{2\pi(n+\frac{1}{2})}{\beta}$ is a fermionic Matsubara frequency with $\beta = \frac{1}{T}$ being the inverse temperature. The k_x dependence is suppressed, as the dispersion is only a function of l.

To model the effect of impurities in the system, the fermions obtain a finite lifetime τ (a more complete treatment of impurity scattering is given in chapter 3.1). It will manifest as an imaginary contribution to the self-energy

$$\Sigma_l(i\omega_n) = -\frac{\mathrm{i}\,\mathrm{sgn}(\omega_n)}{2\tau}, \tag{2.19}$$

which appears in the Green's function as

$$G_l(i\omega_n) = \frac{1}{\mathrm{i}\omega_n - \varepsilon_l - \Sigma_l(i\omega_n)}. \tag{2.20}$$

For further calculations, the retarded/advanced Green's functions are required, which are obtained by taking the analytic continuation $\omega_n \to \omega \pm \mathrm{i}\delta$, with δ being a small, positive constant. In this case, the Green's functions take the form:

$$G_l^{\pm}(\omega) = \frac{1}{\omega - \varepsilon_l \mp \mathrm{i}\frac{1}{2\tau}}. \tag{2.21}$$

2.3 De Haas-van Alphen effect

The de Haas-van Alphen effect denotes oscillations of thermodynamic quantities, like magnetization or magnetic susceptibility, as a function of the inverse magnetic field. To compute those quantities, it is best to use the density of states to obtain the thermodynamic potential, from which observables can be derived by taking appropriate derivatives. This effect was first explained by Lifshitz and Kosevich [8]. I rederive their result using a more general method presented in [18].

The density of states ρ can be obtained directly from the Green's function:

$$\begin{aligned}\rho(\omega) &= -\frac{1}{\pi L_x L_y}\mathrm{Tr}\left[\mathfrak{Im}\, G(\omega)\right] \\ &= -\frac{1}{\pi L_x L_y}\sum_{l,k_x}\frac{\mathfrak{Im}\,\Sigma_l(\omega)}{(\omega - \varepsilon_l - \mathfrak{Re}\,\Sigma_l)^2 + (\mathfrak{Im}\,\Sigma_l)^2}.\end{aligned} \tag{2.22}$$

The sum over k_x is trivial and simply produces a factor N_Φ:

$$\rho(\omega) = -\frac{eB}{2\pi^2}\sum_{l}\frac{\mathfrak{Im}\,\Sigma_l(\omega)}{(\omega - \varepsilon_l - \mathfrak{Re}\,\Sigma_l)^2 + (\mathfrak{Im}\,\Sigma_l)^2}. \tag{2.23}$$

The case of interest is that of the l-independent self-energy. Then, the sum over l can be evaluated using the Poisson summation formula (for proof, see appendix A)

$$\sum_{n=a}^{\infty} f(n) = \sum_{k=-\infty}^{\infty}\int_a^{\infty} dx\, \mathrm{e}^{2\pi \mathrm{i} k x} f(x). \tag{2.24}$$

Defining $\epsilon = \frac{\omega}{\omega_c}$, $w = \frac{\mu - \mathfrak{Re}\,\Sigma}{\omega_c}$, $\Gamma = -\frac{\mathfrak{Im}\,\Sigma}{\omega_c}$ and applying the formula, the density of states transforms into

$$\rho(\omega) = \frac{m}{2\pi^2}\sum_{k=-\infty}^{\infty}\int_0^{\infty} dx \frac{|\Gamma|\mathrm{e}^{2\pi \mathrm{i} k x}}{(\epsilon - x - \frac{1}{2} + w)^2 + \Gamma^2}. \tag{2.25}$$

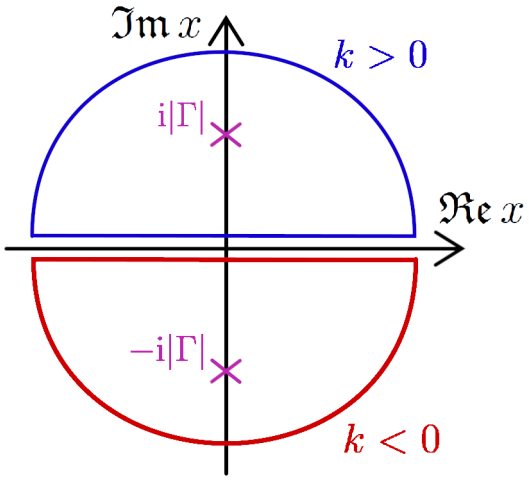

Figure 2.3: The integration contours (in blue and red) used in evaluation of the density of states, and the poles of the integrand (in pink). The arcs are understood to lie at infinity, such that they do not contribute to the integral.

After taking $x \to x + \epsilon + w - \frac{1}{2}$:

$$\rho(\omega) = \frac{m}{2\pi^2} \sum_{k=-\infty}^{\infty} \int_{\frac{1}{2}-\epsilon-w}^{\infty} dx \frac{(-1)^k |\Gamma| \mathrm{e}^{2\pi \mathrm{i} k(x+\epsilon+w)}}{x^2 + \Gamma^2} \tag{2.26}$$

the lower integration bound can be extended to $-\infty$. This step is justified, as in the considered case $w = \frac{\mu}{\omega_c}$ is large. The integral for $k = 0$ is special, as it can be evaluated immediately and gives a non-oscillating contribution to ρ. For $k \neq 0$, the integral can be computed using contour integration. The integrand has two poles at $x = \pm \mathrm{i}|\Gamma|$. The poles and two appropriate contours are depicted in figure 2.3. The choice of contour depends on the sign of k, to ensure $\mathrm{e}^{\mathrm{i}kx}$ goes to 0 at the closing semicircle. After computing the integrals, the density of states is

$$\begin{aligned} \rho(\omega) &= \frac{m}{2\pi} \sum_{k=-\infty}^{\infty} (-1)^k \mathrm{e}^{2\pi \mathrm{i} k(\epsilon+w)} R_D^k \\ &= \frac{m}{2\pi} \left(1 + 2 \sum_{k=1}^{\infty} (-1)^k \cos\left[2\pi k(\epsilon + w)\right] R_D^k \right), \end{aligned} \tag{2.27}$$

where I introduced the Dingle damping factor

$$R_D = \exp\left(-\frac{2\pi |\,\mathfrak{Im}\, \Sigma|}{\omega_c} \right). \tag{2.28}$$

Now, I can calculate the thermodynamic potential using

$$\begin{aligned}\Omega &= -T\sum_{\text{states}}\log\left(1+\mathrm{e}^{-\beta E}\right) = -T\int_{-\infty}^{\infty} dE\,\rho(E)\log\left(1+\mathrm{e}^{-\beta E}\right)\\ &= -\int_{-\infty}^{\infty} dE\,n_F(E)N(E),\end{aligned} \tag{2.29}$$

where I defined the number of states below energy E as

$$N(E) = \int_{-\infty}^{E} d\omega\,\rho(\omega). \tag{2.30}$$

When the self energy has the form Eq. (2.19), N is easily computed and yields (keeping only oscillatory terms)

$$N(\omega) = \frac{eB}{2\pi^2}\sum_{k=1}^{\infty}\frac{(-1)^k}{k}\sin\left[2\pi k(\epsilon+w)\right]R_D^k. \tag{2.31}$$

Then, using Eq. (2.29) and the imaginary part of an integral formula (proven in the appendix A)

$$\int_{-\infty}^{\infty} dx\frac{\mathrm{e}^{\mathrm{i}\alpha x}}{1+\mathrm{e}^{x}} = -\frac{\mathrm{i}\pi}{\sinh(\pi\alpha)}, \tag{2.32}$$

the thermodynamic potential is shown to be

$$\Omega = \frac{(eB)^2}{4\pi^3 m}\sum_{k=1}^{\infty}\frac{(-1)^k}{k^2}\cos\left(2\pi k\frac{\mu}{\omega_c}\right)R_{LK}\left(\frac{2\pi^2 kT}{\omega_c}\right)R_D^k, \tag{2.33}$$

with the Lifshitz-Kosevich temperature damping factor defined as in Eq. (1.1).

The magnetization is straightforwardly computed by taking a derivative of Ω with respect to the magnetic field. The term where the derivative is taken with respect to B inside of the cosine dominates, as it is proportional to a large factor $\frac{\mu}{\omega_c}$. Keeping only this term I obtain:

$$M = -\frac{\partial\Omega}{\partial B} = -\frac{\mu e}{2\pi^2}\sum_{k=1}^{\infty}\frac{(-1)^k}{k}\sin\left(2\pi k\frac{\mu}{\omega_c}\right)R_{LK}\left(\frac{2\pi^2 kT}{\omega_c}\right)R_D^k. \tag{2.34}$$

At this point, a few qualitative statements on the form of magnetic oscillations can be made. The magnetization oscillates as a function of $\frac{1}{B}$ with frequencies that are integer multiples of $F = \frac{m\mu}{e}$. It can be related to the area of the Fermi sea S as:

$$S = \pi p_F^2 = 2\pi m\mu = 2\pi eF. \tag{2.35}$$

The k-th harmonic is damped with the k-th power of the Dingle factor Eq. (2.28), which grows with increasing disorder. Due to this damping, only the first few harmonics can be observed in experiments. Oscillations are also exponentially damped with increasing temperature according to the Lifshitz-Kosevich factor Eq. (1.1), which is plotted in figure 2.4.

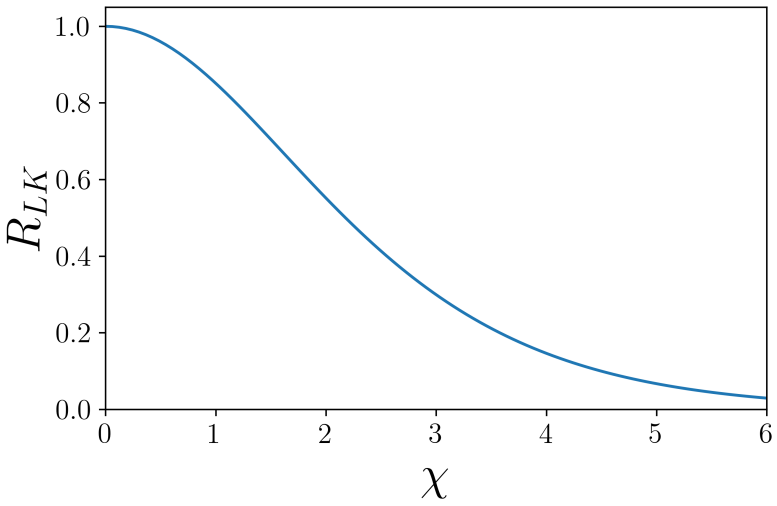

Figure 2.4: The Lifshitz-Kosevich temperature damping factor.

2.4 Shubnikov-de Haas effect

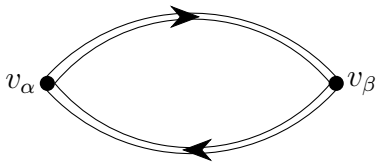

(a) Without vertex corrections.

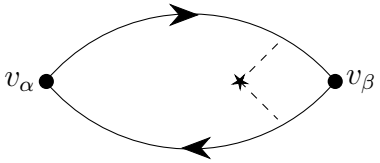

(b) Example vertex correction.

Figure 2.5: Two kinds of contributions to the Kubo formula for conductivity. The diagrams of the type on the right vanish in the considered models.

The Shubnikov-de Haas effect denotes the magnetic oscillations of conductivity. To show it, I need the Kubo-Bastin formula for conductivity in the presence of a magnetic field derived in [24]. Here, I rederive the result starting

from the general Kubo formula

$$\sigma_{\alpha\beta}(\omega) = \sigma^g_{\alpha\beta}(\omega) - \mathrm{i}\frac{e^2}{\omega}S_{\alpha\beta}(\omega), \tag{2.36}$$

where the first term is the gauge term

$$\sigma^g_{\alpha\beta}(\omega) = -\frac{\mathrm{i}Ne^2\delta_{\alpha\beta}}{m\omega}. \tag{2.37}$$

$S_{\alpha\beta}(\omega)$ is obtained by taking the analytic continuation $\mathrm{i}\omega_n \to \omega + \mathrm{i}\delta$ of

$$S_{\alpha\beta}(\mathrm{i}\omega_n) = T\sum_{\nu_n} \mathrm{Tr}\left[v_\alpha G(\mathrm{i}\nu_n) v_\beta G(\mathrm{i}\nu_n + \mathrm{i}\omega_n)\right], \tag{2.38}$$

where v_α is the velocity operator in the α direction. The above formula in terms of diagrams is a bubble of two Green's functions with two insertions of the velocity operator, as in figure 2.5a. There are no vertex corrections (i.e. diagrams with interaction/impurity lines connecting the two Green's functions as in figure 2.5b) contributing to the conductivity in the case of momentum-independent interactions and impurity scattering. To show this, note that the velocity operators are related to the momentum and position operators $\hat{p}$, $\hat{x}$ of the harmonic oscillator the energy levels of which are the Landau levels. Looking at transformation Eq. (2.12), it is clear that $v_x = \frac{k_x}{m} = \frac{\hat{x}eB}{m}$ and $v_y = \frac{k_y}{m} = \frac{\hat{p}}{m}$. Then introducing the Landau level ladder operators as

$$a = \sqrt{\frac{m\omega_c}{2}}\left(\hat{x} + \mathrm{i}\frac{\hat{p}}{m\omega_c}\right); \tag{2.39}$$

$$a^\dagger = \sqrt{\frac{m\omega_c}{2}}\left(\hat{x} - \mathrm{i}\frac{\hat{p}}{m\omega_c}\right), \tag{2.40}$$

the velocity operators can be expressed as

$$v_x = \sqrt{\frac{\omega_c}{2m}}\left(a^\dagger + a\right); \tag{2.41}$$

$$v_y = \mathrm{i}\sqrt{\frac{\omega_c}{2m}}\left(a^\dagger - a\right). \tag{2.42}$$

The momentum k_x is left unchanged by the velocity operators. Therefore, any diagram with a vertex correction is proportional to an integral

$$\int dk_x \psi^\dagger_l\left(y - \frac{k_x}{eB}\right)\psi_{l-1}\left(y - \frac{k_x}{eB}\right) = 0 \tag{2.43}$$

and thus vanishes.

The Matsubara sum in Eq. (2.38) can be evaluated by replacing it with an integral with the Fermi-Dirac distribution. One has to proceed with caution, as the integrand has two discontinuities – one on the real line and another on the line with imaginary part equal to $-\mathrm{i}\omega_n$ – because the imaginary part of the self-energy Eq. (2.19) changes sign at these values. The three necessary contours are depicted in figure 2.6.

After simplifying and taking the analytic continuation, the formula is transformed into

$$S_{\alpha\beta}(\omega) = \int_{-\infty}^{\infty} \frac{d\nu}{2\pi}[-2n_F(\nu)]\mathrm{Tr}\left[v_\alpha \,\mathfrak{Im}\, G(\nu) v_\beta G^+(\nu+\omega) + v_\alpha G^-(\nu) v_\beta \,\mathfrak{Im}\, G(\nu+\omega)\right]. \tag{2.44}$$

In the static limit $\omega \to 0$, this expression can be treated perturbatively in $\frac{\omega}{\omega_c}$. Using

$$\mathfrak{Im}\, G = \frac{1}{2\mathrm{i}}(G^+ - G^-) \tag{2.45}$$

the leading order term can be represented as

$$S_{\alpha\beta}(0) = \mathrm{i}\int_{-\infty}^{\infty} \frac{d\nu}{2\pi}[-2n_F(\nu)]\mathrm{Tr}\left[v_\alpha G^+(\nu) v_\beta G^+(\nu) - v_\alpha G^-(\nu) v_\beta G^-(\nu)\right]. \tag{2.46}$$

It has to cancel with the gauge term Eq. (2.37) for the conductivity Eq. (2.36) to be finite. Indeed, using the commutation relation of the position operator r_α and the inverse Green's function

$$v_\alpha = -\mathrm{i}[r_\alpha, H] = \mathrm{i}[r_\alpha, G^{-1}] \tag{2.47}$$

the integral can be brought to a form

$$S_{\alpha\beta}(0) = \delta_{\alpha\beta}\int_{-\infty}^{\infty} \frac{d\nu}{2\pi\mathrm{i}}[-2n_F(\nu)]\mathrm{Tr}\left[G^+(\nu) - G^-(\nu)\right] = -\frac{N\delta_{\alpha\beta}}{m} \tag{2.48}$$

which cancels with the gauge term exactly.

Keeping only the term independent of ω (as all the others are proportional to ω and thus vanish), the conductivity takes the form

$$\sigma_{\alpha\beta}(0) = \frac{\mathrm{i}e^2}{\pi}\int_{-\infty}^{\infty} d\nu\, n_F(\nu)\mathrm{Tr}\Big[v_\alpha \,\mathfrak{Im}\, G(\nu) v_\beta G'^+(\nu) - v_\alpha G'^-(\nu) v_\beta \,\mathfrak{Im}\, G(\nu)\Big], \tag{2.49}$$

where $G'^{\pm}$ are the derivatives of the retarded/advanced Green's function with respect to energy.

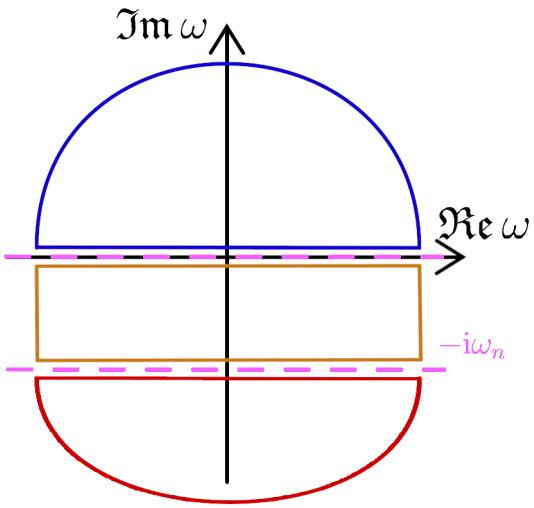

Figure 2.6: The integral contours used in evaluation of the conductivity (in blue, orange and red) and the branch cuts of the integrand (in pink). The arcs at the top and bottom as well as the lines on the left and right are understood to lie at infinity, such that they do not contribute to the integral.

2.4.1 Longitudinal conductivity

In the longitudinal conductivity, Eq. (2.49) can be simplified due to the cyclicity of the trace and formula Eq. (2.45). It is transformed like

$$\begin{aligned}\sigma_{\alpha\alpha} =& \frac{\mathrm{i}e^2}{\pi}\int_{-\infty}^{\infty} d\nu\, n_F(\nu)\mathrm{Tr}\left[v_\alpha\, \mathfrak{Im}\, G(\nu) v_\alpha \left(G'^{+}(\nu) - G'^{-}(\nu)\right)\right] \\ =& -\frac{2e^2}{\pi}\int_{-\infty}^{\infty} d\nu\, n_F(\nu)\mathrm{Tr}\left[v_\alpha\, \mathfrak{Im}\, G(\nu) v_\alpha\, \mathfrak{Im}\, G'(\nu)\right]. \end{aligned} \tag{2.50}$$

Using integration by parts, the integral can be carried out in two steps as

$$\sigma_{\alpha\alpha} = \int_{-\infty}^{\infty} d\omega\, [-n'_F(\omega)]\hat{\sigma}_{\alpha\alpha}(\omega); \tag{2.51}$$

$$\hat{\sigma}_{\alpha\alpha}(\omega) = -\frac{e^2}{\pi}\mathrm{Tr}\left[v_\alpha\, \mathfrak{Im}\, G(\omega) v_\alpha\, \mathfrak{Im}\, G(\omega)\right], \tag{2.52}$$

where $-n'_F(E) = \frac{\beta}{4\cosh^2(\frac{\beta E}{2})}$ is the derivative of the Fermi-Dirac distribution. The trace in the conductivity kernel Eq. (2.52) contains a trivial momentum

sum which produces a prefactor of N_Φ. Then, the trace over Landau levels can be performed as

$$\hat{\sigma}_{\alpha\alpha}(\omega) = -\frac{e^2 N_\Phi}{\pi L_x L_y} \sum_{l,l'} \langle l| \, v_\alpha \, |l'\rangle \, \mathfrak{Im}\, G_{l'}(\omega) \, \langle l'| \, v_\alpha \, |l\rangle \, \mathfrak{Im}\, G_l(\omega). \tag{2.53}$$

The matrix elements of the velocity operators are

$$\langle l| \, v_x \, |l'\rangle = \sqrt{\frac{\omega_c}{2m}} \, \langle l| \, a^\dagger + a \, |l'\rangle = \sqrt{\frac{\omega_c}{2m}} \left(\sqrt{l}\delta_{l,l'+1} + \sqrt{l+1}\delta_{l,l'-1} \right); \tag{2.54}$$

$$\langle l| \, v_y \, |l'\rangle = \mathrm{i}\sqrt{\frac{\omega_c}{2m}} \, \langle l| \, a^\dagger - a \, |l'\rangle = \mathrm{i}\sqrt{\frac{\omega_c}{2m}} \left(\sqrt{l}\delta_{l,l'+1} - \sqrt{l+1}\delta_{l,l'-1} \right). \tag{2.55}$$

Using Eq. (2.54), one of the LL sums in Eq. (2.53) can be resolved, giving

$$\hat{\sigma}_{xx}(\omega) = \frac{e^2 N_\Phi \omega_c}{\pi m L_x L_y} \sum_{l=1}^{\infty} l \, \mathfrak{Im}\, G_l(\omega) \, \mathfrak{Im}\, G_{l-1}(\omega). \tag{2.56}$$

To compute the remaining sum, the same strategy as for the density of states Eq. (2.23) can be employed: firstly, the sum is changed into an integral with the Poisson summation formula Eq. (2.24). Then, after a change of variables $l \to l - \frac{\mu}{\omega_c}$, the lower integration boundary is extended like $-\frac{\mu}{\omega_c} \to -\infty$. The integral is evaluated using contour integration – the choice of the contour depends on the sign of k. The integrand has four poles at $\pm\mathrm{i}|\Gamma|, 1 \pm \mathrm{i}|\Gamma|$, depending on the contour the poles in the lower/upper half of the complex plane have to be included. Finally, the kernel turns out to equal

$$\hat{\sigma}_{xx}(\omega) = \sigma_0 \frac{(\epsilon + w)|\Gamma|}{1 + 4\Gamma^2} \left[1 + 2 \sum_{k=1}^{\infty} (-1)^k \cos[2\pi k(\epsilon + w)] R_D^k \right] \tag{2.57}$$

with $\sigma_0 = \frac{2e^2}{\pi}$ and $\epsilon = \frac{\omega}{\omega_c}$, $w = \frac{\mu - \mathfrak{Re}\,\Sigma}{\omega_c}$ as in the calculation of the density of states. In the simplest case Eq. (2.19), the self-energy does not depend on ω and the integral Eq. (2.51) can be evaluated using formula Eq. (2.32) integrated by parts

$$\int_{-\infty}^{\infty} dx \frac{\mathrm{e}^{\mathrm{i}\alpha x}}{\cosh^2(x)} = \frac{\alpha\pi}{\sinh(\alpha\pi)}. \tag{2.58}$$

Keeping only oscillating terms with the highest power of $\frac{\mu}{\omega_c}$, the longitudinal conductivity takes the form

$$\sigma_{xx} = \sigma_0 \frac{\mu|\Gamma|}{\omega_c(1 + 4\Gamma^2)} \left[1 + 2 \sum_{k=1}^{\infty} (-1)^k \cos\left(2\pi k \frac{\mu}{\omega_c} \right) R_{LK} \left(\frac{2\pi^2 kT}{\omega_c} \right) R_D^k \right]. \tag{2.59}$$

Conductivity oscillations have similar features to oscillations of magnetization Eq. (2.34). The only difference is the amplitude, which scales linearly with the chemical potential μ and depends on the scattering rate through Γ.

2.4.2 Transversal conductivity

The Kubo formula for transversal conductivity

$$\sigma_{xy} = \frac{\mathrm{i}e^2}{\pi}\int_{-\infty}^{\infty} d\nu\, n_F(\nu)\mathrm{Tr}\left[v_x\,\mathfrak{Im}\,G(\nu)v_yG'^{+}(\nu) - v_xG'^{-}(\nu)v_y\,\mathfrak{Im}\,G(\nu)\right] \tag{2.60}$$

needs to be transformed to make further calculations feasible. I use the simplification developed by Smrčka and Streda [25, 26]. Using the commutation relation of the position operator r_α and the inverse Green's function

$$v_\alpha = [r_\alpha, H] = [r_\alpha, G^{-1}] \tag{2.61}$$

the trace in the integrand can be split into two parts

$$\mathrm{Tr}\left[v_x\,\mathfrak{Im}\,G(\epsilon)v_yG'^{+}(\epsilon) - v_xG'^{-}(\epsilon)v_y\,\mathfrak{Im}\,G(\epsilon)\right] = \frac{1}{2}\frac{\partial}{\partial\epsilon}\mathfrak{A}(\epsilon) + \mathfrak{B}(\epsilon), \tag{2.62}$$

where $\mathfrak{A}(\epsilon)$ and $\mathfrak{B}(\epsilon)$ are

$$\mathfrak{A}(\epsilon) = \mathrm{i}\mathrm{Tr}\left[v_x\,\mathfrak{Im}\,G(\epsilon)v_yG^{+}(\epsilon) - v_xG^{-}(\epsilon)v_y\,\mathfrak{Im}\,G(\epsilon)\right]; \tag{2.63}$$

$$\mathfrak{B}(\epsilon) = \frac{1}{2}\mathrm{Tr}\left[\frac{\partial\,\mathfrak{Im}\,G(\epsilon)}{\partial\epsilon}(r_\alpha v_\beta - r_\beta v_\alpha)\right]. \tag{2.64}$$

Keeping in mind that $G(\epsilon)$ depends on ϵ in the same way as on B save for a prefactor, $\mathfrak{B}(\epsilon)$ can be further rewritten as

$$\mathfrak{B}(\epsilon) = \frac{1}{e}\frac{\partial}{\partial B}\mathrm{Tr}\,\mathfrak{Im}\,G(\epsilon). \tag{2.65}$$

After integration by parts, I split Eq. (2.60) into σ^I_{xy} – a part with $\mathfrak{A}$ and σ^{II}_{xy} – a part with $\mathfrak{B}$ to express the transversal conductivity like

$$\sigma_{xy} = \int_{-\infty}^{\infty} d\omega\,[-n'_F(\omega)]\left(\hat{\sigma}^I_{xy}(\omega) + \hat{\sigma}^{II}_{xy}(\omega)\right); \tag{2.66}$$

$$\hat{\sigma}^{\mathrm{I}}_{xy}(\omega) = \frac{\mathrm{i}e^2}{2\pi}\mathrm{Tr}\left[v_x\,\mathfrak{Im}\,G(\omega)v_yG^{+}(\omega) - v_xG^{-}(\omega)v_y\,\mathfrak{Im}\,G(\omega)\right]; \tag{2.67}$$

$$\hat{\sigma}^{\mathrm{II}}_{xy}(\omega) = e\frac{\partial N(\omega)}{\partial B}, \tag{2.68}$$

where $N(\omega)$ is the number of states below energy ω as defined in Eq. (2.31).

With the help of the matrix elements of the velocity operators Eq. (2.54) and Eq. (2.55), the first part of the transversal conductivity kernel Eq. (2.67) can be expressed as

$$\begin{aligned}\hat{\sigma}^{\mathrm{I}}_{xy}(\omega) &= \frac{e^2 N_\Phi \omega_c}{2\pi m L_x L_y} \sum_l l \left[\mathfrak{Im}\, G_{l-1}(\omega)\, \mathfrak{Re}\, G_l(\omega) - \mathfrak{Re}\, G_{l-1}(\omega)\, \mathfrak{Im}\, G_l(\omega)\right] \\ &= -\frac{1}{2|\Gamma|}\hat{\sigma}_{xx}(\omega) \\ &= -\frac{\sigma_0}{2}\frac{(\epsilon+w)}{1+4\Gamma^2}\left[1+2\sum_{k=1}^{\infty}(-1)^k \cos[2\pi k(\epsilon+w)]R_D^k\right]. \end{aligned} \tag{2.69}$$

As for the second part of the kernel Eq. (2.68), after derivating Eq. (2.31) with respect to B, I get

$$\hat{\sigma}^{\mathrm{II}}_{xy}(\omega) = -\frac{\sigma_0}{2}(\epsilon+w)\sum_{k=1}^{\infty}(-1)^k \cos[2\pi k(\epsilon+w)]R_D^k. \tag{2.70}$$

The two contributions can be combined into the transversal resistivity kernel

$$\hat{\sigma}_{xy}(\omega) = -\frac{\sigma_0}{2}\frac{(\epsilon+w)}{1+4\Gamma^2}\left[1+(3+4\Gamma^2)\sum_{k=1}^{\infty}(-1)^k \cos[2\pi k(\epsilon+w)]R_D^k\right] \tag{2.71}$$

and then integrated with the derivative of the Fermi-Dirac distribution to obtain the oscillating part of the transversal conductivity

$$\begin{aligned}\sigma_{xy} = &-\frac{\sigma_0}{2}\frac{\mu}{\omega_c(1+4\Gamma^2)} \\ &\times\left[1+(3+4\Gamma^2)\sum_{k=1}^{\infty}(-1)^k \cos\left(2\pi k\frac{\mu}{\omega_c}\right) R_{LK}\left(\frac{2\pi^2 kT}{\omega_c}\right) R_D^k\right].\end{aligned} \tag{2.72}$$

The oscillations have a familiar form – they differ from longitudinal conductivity oscillations Eq. (2.59) only in the dependence of the prefactor on Γ. The following relations hold:

$$\sigma^{\mathrm{non-osc}}_{xx} = -\,2|\Gamma|\sigma^{\mathrm{non-osc}}_{xy}; \tag{2.73}$$

$$\sigma^{\mathrm{osc}}_{xx} = -\,\frac{2|\Gamma|}{3+4\Gamma^2}\sigma^{\mathrm{osc}}_{xy}. \tag{2.74}$$

Chapter 3

Interaction-induced combination frequencies

3.1 Feynman rules

To see the effects of interactions on the QO spectrum, it is necessary to treat them microscopically. I introduce two new terms to the Hamiltonian, one modeling scattering on impurities, and the other electronic interactions

$$H_{\text{imp}} = \sum_{i=1}^{N_{\text{imp}}} \int d^2\boldsymbol{r}\, u(\boldsymbol{r} - \boldsymbol{R}_i)\phi^\dagger(\boldsymbol{r})\phi(\boldsymbol{r}); \tag{3.1}$$

$$H_{\text{int}} = \int d^2\boldsymbol{r} \int d^2\boldsymbol{r}'\, V(\boldsymbol{r} - \boldsymbol{r}')\phi^\dagger(\boldsymbol{r})\phi^\dagger(\boldsymbol{r}')\phi(\boldsymbol{r}')\phi(\boldsymbol{r}). \tag{3.2}$$

The system contains N_{imp} impurities at random positions $\boldsymbol{R}_i$. The electrons scatter on impurities with potential u and interact with potential V. Later, both potentials will be set to delta functions for simplicity, but for now I proceed with a general position dependence.

After transforming the fields with Eq. (2.12), as well as Fourier transforming u and V like

$$u(\mathbf{r}) = \frac{1}{L_x L_y} \sum_{\mathbf{q}} \mathrm{e}^{\mathrm{i}\mathbf{q}\cdot\mathbf{r}} u_{\mathbf{q}}; \tag{3.3}$$

$$V(\mathbf{r}) = \frac{1}{L_x L_y} \sum_{\mathbf{q}} \mathrm{e}^{\mathrm{i}\mathbf{q}\cdot\mathbf{r}} V_{\mathbf{q}}, \tag{3.4}$$

the Hamiltonian terms take the form

$$H_{\text{imp}} = \sum_{l,l',k_x} \frac{1}{L_x L_y} \sum_{\mathbf{q}} \sum_{i=1}^{N_{\text{imp}}} \mathrm{e}^{-\mathrm{i}\mathbf{q}\cdot\mathbf{R}_i} u_{\mathbf{q}} \times \int dy\, \mathrm{e}^{\mathrm{i}q_y y} \psi^*_{l'} \left(y - \frac{k_x + q_x}{eB} \right) \psi_l \left(y - \frac{k_x}{eB} \right) \phi^\dagger_{k_x+q_x,l',\sigma} \phi_{k_x,l,\sigma}; \quad (3.5)$$

$$\begin{aligned} H_{\text{int}} = & \sum_{k_x,k'_x} \sum_{l_1,l_2,l_3,l_4} \frac{1}{L_x L_y} \sum_{\mathbf{q}} V_{\mathbf{q}} \\ & \times \int dy\, \mathrm{e}^{\mathrm{i}q_y y} \psi^*_{l_2} \left(y - \frac{k_x + q_x}{eB} \right) \psi_{l_1} \left(y - \frac{k_x}{eB} \right) \\ & \times \int dy'\, \mathrm{e}^{-\mathrm{i}q_y y'} \psi^*_{l_4} \left(y' - \frac{k'_x - q_x}{eB} \right) \psi_{l_3} \left(y' - \frac{k'_x}{eB} \right) \\ & \times \phi^\dagger_{k_x+q_x,l_2} \phi^\dagger_{k'_x-q_x,l_4} \phi_{k_x,l_1} \phi_{k'_x,l_3}. \end{aligned} \quad (3.6)$$

It is apparent that the integral

$$\mathcal{I}(k_x, \mathbf{q}, l, l') = \int dy \mathrm{e}^{\mathrm{i}q_y y} \psi^*_{l'} \left(y - \frac{k_x + q_x}{eB} \right) \psi_l \left(y - \frac{k_x}{eB} \right) \quad (3.7)$$

is crucial in computations with the above Hamiltonian. It can be evaluated analytically (see appendix A) and yields

$$\mathcal{I}(k_x, \mathbf{q}, l, l') = \sqrt{\frac{l!}{l'!}} \left(\frac{-q_x + \mathrm{i}q_y}{\sqrt{2eB}} \right)^{l'-l} \mathrm{e}^{\mathrm{i}q_y \frac{q_x+2k_x}{2eB}} \mathrm{e}^{-\frac{\mathbf{q}^2}{4eB}} L_l^{l'-l} \left(\frac{\mathbf{q}^2}{2eB} \right), \quad (3.8)$$

where $L_n^m(x)$ is the generalized Laguerre polynomial. In terms of $\mathcal{I}$, the Hamiltonian can be expressed as

$$H_{\text{imp}} = \sum_{l,l',k_x} \frac{1}{L_x L_y} \sum_{\mathbf{q}} \sum_{i=1}^{N_{\text{imp}}} \mathrm{e}^{-\mathrm{i}\mathbf{q}\cdot\mathbf{R}_i} u_{\mathbf{q}} \mathcal{I}(k_x, \mathbf{q}, l, l') \phi^\dagger_{k_x+q_x,l'} \phi_{k_x,l}; \quad (3.9)$$

$$\begin{aligned} H_{\text{int}} = & \sum_{k_x,k'_x} \sum_{l_1,l_2,l_3,l_4} \frac{1}{L_x L_y} \sum_{\mathbf{q}} V_{\mathbf{q}} \mathcal{I}(k_x, \mathbf{q}, l_1, l_2) \mathcal{I}(k'_x, -\mathbf{q}, l_3, l_4) \\ & \times \phi^\dagger_{k_x+q_x,l_2} \phi^\dagger_{k'_x-q_x,l_4} \phi_{k_x,l_1} \phi_{k'_x,l_3}. \end{aligned} \quad (3.10)$$

From this form of H, the Feynman rules can be immediately read off as

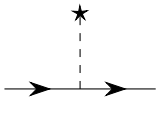

$$= \frac{1}{L_x L_y} \sum_{q_y} \sum_{i=1}^{N_{\text{imp}}} \mathrm{e}^{-\mathrm{i}\mathbf{q}\cdot\mathbf{R}_i} u_{\mathbf{q}} \mathcal{I}\left(k_x, \mathbf{q}, l, l'\right); \tag{3.11}$$

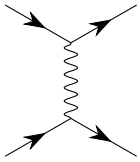

$$= \frac{1}{\beta L_x L_y} \sum_{\omega_n, q_y} V_{\mathbf{q}} \mathcal{I}\left(k_x, \mathbf{q}, l_1, l_2\right) \mathcal{I}\left(k'_x, -\mathbf{q}, l_3, l_4\right). \tag{3.12}$$

3.2 Self-energy

Using the derived Feynman rules, I compute diagrams to second order in impurity scattering and to first order in interactions. I assume the system is self-averaging, therefore I can average over impurity positions $\boldsymbol{R}_i$ to obtain a self-energy that is independent of them.

The lowest order impurity diagram is

$$\begin{aligned} &= \frac{n_{\text{imp}}}{L_x L_y} \sum_{q_y} \int d^2\mathbf{R}\, \mathrm{e}^{-\mathrm{i}\mathbf{q}\cdot\mathbf{R}} u_{\mathbf{q}} \int dy\, \mathrm{e}^{\mathrm{i}q_y y} \psi^*_{l'}\left(y - \frac{k_x + q_x}{eB}\right) \psi_l\left(y - \frac{k_x}{m\omega_c}\right) \\ &= n_{\text{imp}} u_0 \delta_{k_x, k'_x} \delta_{l,l'}, \end{aligned} \tag{3.13}$$

where $n_{\text{imp}} = \frac{N_{\text{imp}}}{L_x L_y}$ is the impurity concentration. The diagram is a constant independent of incoming energy, momentum and LL index. It is also diagonal in all quantum numbers. The next lowest-order contribution is a diagram corresponding to two scattering events on a single impurity.

$$\begin{aligned} &= \frac{n_{\text{imp}}}{L_x^2 L_y^2} \sum_{q_x, q_{1y}, q_{2y}, r} \int d^2\mathbf{R} \mathrm{e}^{-\mathrm{i}(q_x - k_x + k'_x - q_x)X - i(q_{1y} + q_{2y})Y} u_{q_x - k_x, q_{1y}} \\ &\quad \times u_{k'_x - q_x, q_{2y}} \mathcal{I}\left(k_x, q_x - k_x, q_{1y}, l, r\right) \mathcal{I}\left(q_x, k'_x - q_x, q_{2y}, r, l'\right) G_r^0 \\ &= \frac{n_{\text{imp}} \delta_{k_x, k'_x}}{(2\pi)^2} \sum_r \int d^2\mathbf{q} |u_{\mathbf{q}}|^2 \sqrt{\frac{l!}{l'!}} (-1)^{r-l} \left(\frac{q_x - \mathrm{i}q_y}{\sqrt{2eB}}\right)^{l'-l} \mathrm{e}^{-\frac{\boldsymbol{q}^2}{2eB}} \\ &\quad \times L_r^{l'-r}\left(\frac{\boldsymbol{q}^2}{2eB}\right) L_l^{r-l}\left(\frac{\boldsymbol{q}^2}{2eB}\right) G_r^0. \end{aligned} \tag{3.14}$$

After a change into polar coordinates $q_x - \mathrm{i}q_y \to q\mathrm{e}^{-\mathrm{i}\varphi}$, I notice that the only dependence of the integrand on φ is through a factor $\mathrm{e}^{\mathrm{i}(l-l')\varphi}$ (provided $u_{\boldsymbol{q}}$ depends only on the magnitude of $\boldsymbol{q}$). Then, the integral over φ can be evaluated and gives a factor of $2\pi\delta_{l,l'}$ - the diagram is diagonal in the LL index. It equals to

$$= \frac{n_{\mathrm{imp}}\delta_{k_x,k_x'}\delta_{l,l'}}{2\pi} \sum_r \int_0^\infty dq\, q|u_q|^2 (-1)^{r-l} \mathrm{e}^{-\frac{q^2}{2eB}} L_r^{l-r}\left(\frac{q^2}{2eB}\right) L_l^{r-l}\left(\frac{q^2}{2eB}\right) G_r^0. \tag{3.15}$$

To make further progress, I have to specify the form of the scattering potential. I choose the point-like scattering potential, as this simple case already yields the desired result (a more realistic case of Gaussian extended impurities is discussed in appendix C). In momentum space, it is expressed as

$$u_{\boldsymbol{q}} = u_0. \tag{3.16}$$

Then, the second-order diagram simplifies to

$$= \frac{n_{\mathrm{imp}} u_0^2 eB \delta_{k_x,k_x'}\delta_{l,l'}}{2\pi} \sum_r G_r^0. \tag{3.17}$$

The first considered interaction contribution is the Hartree diagram

$$\begin{aligned}
&= \frac{1}{\beta L_x L_y} \sum_{\omega_n,p_x,q_y,r} V_{0,q_y} \mathcal{I}\left(k_x,0,q_y,l,l'\right) \mathcal{I}\left(p_x,0,-q_y,r,r\right) G_r^0(\mathrm{i}\omega_n) \\
&= \frac{1}{\beta L_x L_y} \sum_{\omega_n,p_x,q_y,r} V_{0,q_y} \sqrt{\frac{l!}{l'!}} \left(-\mathrm{i}q_y\right)^{l'-l} \mathrm{e}^{\frac{\mathrm{i}q_y}{eB}(k_x-p_x)} \mathrm{e}^{-\frac{q_y^2}{2eB}} \\
&\quad \times L_l^{l'-l}\left(\frac{q_y^2}{2eB}\right) L_r^0\left(\frac{q_y^2}{2eB}\right) G_r^0(\mathrm{i}\omega_n) \\
&= \frac{V_0 eB\delta_{l,l'}}{2\pi\beta} \sum_{r,\omega_n} G_r^0(\mathrm{i}\omega_n).
\end{aligned} \tag{3.18}$$

In going from the second to third line, I integrated over p_x to obtain $\delta_{q_y,0}$, which requires $l = l'$ for the diagram to be nonzero.

The second contribution at this order is the Fock diagram

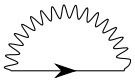

$$= -\frac{1}{\beta L_x L_y} \sum_{\mathbf{q},r,\omega_n} V_{\mathbf{q}} \mathcal{I}\left(k_x, \mathbf{q}, l, r\right) \mathcal{I}\left(k_x + q_x, -\mathbf{q}, r, l'\right) G_r^0(\mathrm{i}\omega_n)$$

$$= -\frac{\delta_{k_x,k_x'}\delta_{l,l'}}{2\pi\beta} \sum_{r,\omega_n} \int_0^\infty dq\, q V_q (-1)^{r-l} \mathrm{e}^{-\frac{\boldsymbol{q}^2}{2eB}}$$

$$\times L_r^{l-r}\left(\frac{q^2}{2eB}\right) L_l^{r-l}\left(\frac{q^2}{2eB}\right) G_r^0(\mathrm{i}\omega_n), \tag{3.19}$$

which has the same form as Eq. (3.15), only summed over the Matsubara frequency. In further considerations, I take a constant $V_q = V_0$, corresponding to the electrons interacting with a delta potential (possibility of proceeding with the Coulomb interactions is discussed in appendix C). Then, the diagram simplifies to

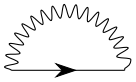

$$= -\frac{V_0 eB \delta_{k_x,k_x'}\delta_{l,l'}}{2\pi\beta} \sum_{r,\omega_n} G_r^0(\mathrm{i}\omega_n). \tag{3.20}$$

The Hartree and Fock diagrams are similar to the impurity contribution Eq. (3.15), but they are summed over the Matsubara frequency in the Green's function. The disparity will turn out to be crucial, as it ensures the diagrams are purely real. For the considered model, the Hartree and Fock diagrams differ only by the sign. However, this is not the case in general. When electron spin is included, the absolute value of the Hartree diagram is twice as big as of the Fock diagram. When one considers momentum-dependent interactions like in appendix C, the Hartree diagram does not change, but the Fock diagram becomes dependent on the incoming Landau level.

3.3 Multi-band systems and interband scattering

The new oscillation frequencies I expect to obtain are combinations of fundamental frequencies. For that, I naturally require a system with multiple different fundamental frequencies. In terms of the band structure, that means multiple distinct Fermi pockets (or, in three dimensions, multiple extremal cross-sections of the Fermi surface). One particularly simple way of constructing a system with this feature is to consider a multi-band system, where the electrons in different bands have a different dispersion [18]. However to utilize the results of section 3.2, it is important that the electrons

in the different bands have the same wavefunction. This is realized by the following two-band free Hamiltonian

$$H_0 = \sum_{l=0}^{\infty} \sum_{k_x,\lambda} \varepsilon_{l,\lambda}\, \phi^\dagger_{k_x,l,\lambda} \phi_{k_x,l,\lambda}, \tag{3.21}$$

where $\lambda \in \{1,2\}$ is the band index. In further considerations, $\bar{\lambda}$ denotes the band other than λ. The dispersion has the same form but with a band-dependent mass and energy shift

$$\varepsilon_{l,\lambda} = \omega_{c\lambda} \left(l + \frac{1}{2} \right) - W_\lambda \tag{3.22}$$

where $\omega_{c\lambda} = \frac{eB}{m_\lambda}$. To allow the two bands to influence each other, I need to modify the impurity and interaction terms as well. In position space, the most general form they can take is

$$H_{\text{imp}} = \sum_{\lambda} \sum_{i=1}^{N_{\text{imp}}} \int d^2\boldsymbol{r}\, u(\boldsymbol{r} - \boldsymbol{R}_i) \Phi^\dagger(\boldsymbol{r}) \boldsymbol{\Lambda} \Phi(\boldsymbol{r}); \tag{3.23}$$

$$\begin{aligned} H_{\text{int}} = \sum_{\lambda} \int d^2\boldsymbol{r} d^2\boldsymbol{r}' V(\boldsymbol{r} - \boldsymbol{r}') \Big[& \gamma_\lambda \phi^\dagger_\lambda(\boldsymbol{r}) \phi^\dagger_\lambda(\boldsymbol{r}') \phi_\lambda(\boldsymbol{r}') \phi_\lambda(\boldsymbol{r}) \\ & + \eta \phi^\dagger_{\bar{\lambda}}(\boldsymbol{r}) \phi^\dagger_\lambda(\boldsymbol{r}') \phi_\lambda(\boldsymbol{r}') \phi_{\bar{\lambda}}(\boldsymbol{r}) + \theta \phi^\dagger_\lambda(\boldsymbol{r}) \phi^\dagger_{\bar{\lambda}}(\boldsymbol{r}') \phi_\lambda(\boldsymbol{r}') \phi_{\bar{\lambda}}(\boldsymbol{r}) \Big], \end{aligned} \tag{3.24}$$

where I introduced $\Phi(\boldsymbol{r}) = (\phi_1(\boldsymbol{r}), \phi_2(\boldsymbol{r}))^T$ and the band mixing matrix

$$\boldsymbol{\Lambda} = \begin{pmatrix} \sqrt{\alpha_1} & \sqrt{\beta} \\ \sqrt{\beta} & \sqrt{\alpha_2} \end{pmatrix}. \tag{3.25}$$

To treat the terms perturbatively, I need to transform the fields into the Landau level basis like in Eq. (2.12). The impurity and interaction potentials need to be Fourier transformed like in Eq. (3.3). Then, the Hamiltonian is brought into the form

$$H_{\text{imp}} = \sum_{l,l',k_x} \frac{1}{L_x L_y} \sum_{\mathbf{q}} \sum_{i=1}^{N_{\text{imp}}} \mathrm{e}^{-\mathrm{i}\mathbf{q}\cdot\mathbf{R}_i} u_{\mathbf{q}} \mathcal{I}\left(k_x, \mathbf{q}, l, l'\right) \Phi^\dagger_{k_x+q_x,l'} \boldsymbol{\Lambda} \Phi_{k_x,l}; \tag{3.26}$$

$$\begin{aligned} H_{\text{int}} = & \sum_{k_x,k_x',\lambda} \sum_{l_1,l_2,l_3,l_4} \frac{1}{L_x L_y} \sum_{\mathbf{q}} V_{\mathbf{q}} \mathcal{I}\left(k_x, \mathbf{q}, l_1, l_2\right) \mathcal{I}\left(k_x', -\mathbf{q}, l_3, l_4\right) \\ & \times \Big[\gamma_\lambda \phi^\dagger_{k_x+q_x,l_2,\lambda} \phi^\dagger_{k_x'-q_x,l_4,\lambda} \phi_{k_x,l_1,\lambda} \phi_{k_x',l_3,\lambda} \\ & + \eta \phi^\dagger_{k_x+q_x,l_2,\lambda} \phi^\dagger_{k_x'-q_x,l_4,\bar{\lambda}} \phi_{k_x,l_1,\lambda} \phi_{k_x',l_3,\bar{\lambda}} \\ & + \theta \phi^\dagger_{k_x+q_x,l_2,\bar{\lambda}} \phi^\dagger_{k_x'-q_x,l_4,\lambda} \phi_{k_x,l_1,\lambda} \phi_{k_x',l_3,\bar{\lambda}} \Big], \end{aligned} \tag{3.27}$$

where $\Phi_{k_x,l} = (\phi_{k_x,l,1}, \phi_{k_x,l,2})^T$.

The impurity term Eq. (3.26) and its treatment were developed in [18], I rederive it with the addition of the new interaction term Eq. (3.27).

To indicate the new interactions, I introduce two types of vertices: squares for those that change the band index, and circles for those that do not. Then, the elementary Feynman diagrams are:

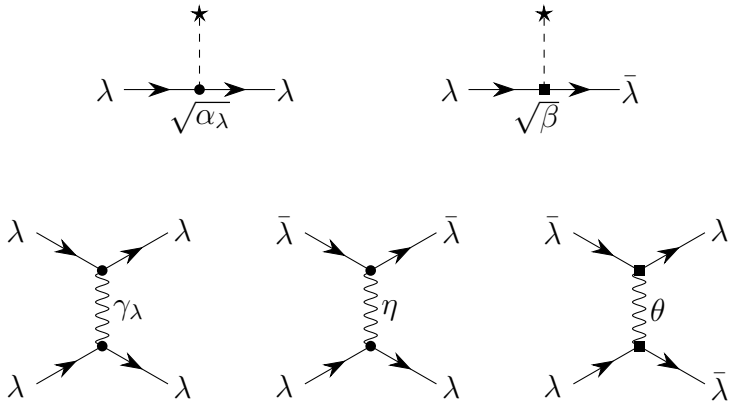

With the new Feynman rules, I can proceed to calculating the self-energy of the multiband system. For that, I use the self-consistent Born approximation. I compute the self-energy contribution with the full Green's functions (i.e. ones already containing the self energy). Then, I solve the resulting self-consistent equations by reinsertion perturbatively in the Dingle factor R_D.

I take diagrams to second order in impurity scattering u_0 and to first order in impurity density n_{imp} and interaction V_0. The relevant diagrams are

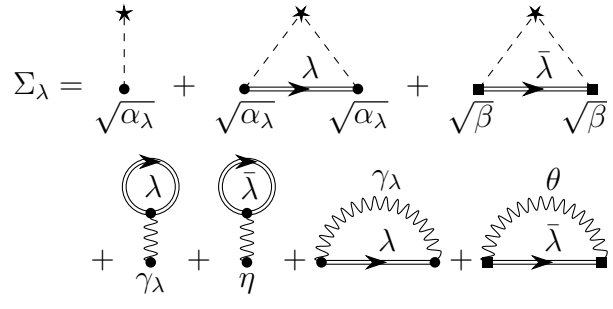

(3.28)

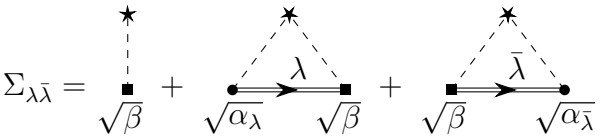

(3.29)

Since the two bands introduce a new degree of freedom, the self energy depends on the band index λ. There are terms non-diagonal in the band index Eq. (3.29), however I neglect them in further considerations in order to make

the analytical calculation feasible. The first-order diagram in u_0 is constant and real, so it can be removed by a redefinition of the energy shifts $W_\lambda \to W_\lambda - n_{\mathrm{imp}} u_0 \sqrt{\alpha_\lambda}$.

To put the diagonal part in an algebraic form, I can use expressions derived in section 3.1. The only changes are the addition of prefactors α, β, γ, η, θ, replacements $m \to m_\lambda$, $\mu \to W_\lambda$ with an appropriate band index and the replacement of free Green's functions with full ones. Then, the diagonal part of the self-energy reads (neglecting the first diagram, which is just a constant real shift)

$$\begin{aligned}\Sigma_\lambda(i\omega_n) =& \frac{eB}{2\pi} \sum_{l=0}^{\infty} \Bigg[n_{\mathrm{imp}} u_0^2 \left(\alpha_\lambda G_{l,\lambda}(i\omega_n) + \beta G_{l,\bar{\lambda}}(i\omega_n) \right) \\ &+ \frac{V_0}{\beta} \sum_{\nu_n} \left(\gamma_\lambda G_{l,\lambda}(i\nu_n) + (\eta - \theta) G_{l,\bar{\lambda}}(i\nu_n) \right) \Bigg], \end{aligned} \tag{3.30}$$

where $G_{l,\lambda}(\mathrm{i}\omega_n) = (\mathrm{i}\omega_n - \varepsilon_{l,\lambda} - \Sigma_\lambda(\mathrm{i}\omega_n))^{-1}$. The LL sums can be evaluated with Poisson summation Eq. (2.24). I employ the same strategy as when calculating the density of states Eq. (2.27): replace the sum over l with an integral, change variables, extend the lower boundary to $-\infty$, and then use contour integration to evaluate the integral. The Green's function has only a single pole, so depending on the sign of k the integral can vanish. After discarding a divergent, non-oscillating real part, the sum equals

$$\sum_l G_l(\mathrm{i}\omega_n) = -\frac{\mathrm{i}\pi \mathrm{sgn}(\omega_n)}{\omega_{c\lambda}} \left[1 + 2 \sum_{k=1}^{\infty} (-1)^k \mathrm{e}^{2\pi \mathrm{i} k \mathrm{sgn}(\omega_n) \frac{\mathrm{i}\omega_n + W_\lambda - \Sigma_\lambda}{\omega_{c\lambda}}} \right]. \tag{3.31}$$

Now, it is suitable to define the Dingle temperature $\pi T_{D\lambda} = \frac{1}{2} n_{\mathrm{imp}} u_0^2 M_\lambda$ as the non-oscillating imaginary part of the self energy. The constants are also redefined as $\tilde{\alpha}_\lambda = \frac{m_\lambda}{M_\lambda}\alpha_\lambda$, $\tilde{\beta}_\lambda = \frac{m_{\bar{\lambda}}}{M_\lambda}\beta$, $\delta = \eta - \theta$, where $M_\lambda = m_\lambda \alpha_\lambda + m_{\bar{\lambda}}\beta$ is the mean effective mass of the two bands. The operator $\mathcal{A}$ is introduced for brevity, its action is $\mathcal{A} f_\lambda = f_{\bar{\lambda}} \mathcal{A}$. Additionally, I define $\Gamma_\lambda = -\frac{\mathfrak{Im}\,\Sigma_\lambda}{\omega_{c\lambda}}$ and $w_\lambda = \frac{W_\lambda - \mathfrak{Re}\,\Sigma_\lambda}{\omega_{c\lambda}}$ in analogy to Γ and w in the single-band case. Then, I split the self energy into a real and imaginary part to get the following

self-consistent equations:

$$\begin{aligned}\mathfrak{Re}\,\Sigma_\lambda =&\pi T_{D\lambda}\left(\tilde{\alpha}_\lambda+\tilde{\beta}_\lambda\mathcal{A}\right)\sum_{k=1}^{\infty}(-1)^k\sin\left(2\pi k w_\lambda\right)\mathrm{e}^{-\frac{2\pi k}{\omega_{c\lambda}}|\omega_n|}\mathrm{e}^{-2\pi k|\Gamma_\lambda|}\\&+\frac{V_0}{\beta}\left(\gamma_\lambda+\delta\mathcal{A}\right)\sum_{\nu_n,k>0}m_\lambda(-1)^k\sin\left(2\pi k w_\lambda\right)\mathrm{e}^{-\frac{2\pi k}{\omega_{c\lambda}}|\nu_n|}\mathrm{e}^{-2\pi k|\Gamma_\lambda|};\end{aligned} \tag{3.32}$$

$$|\,\mathfrak{Im}\,\Sigma_\lambda| =\pi T_{D\lambda}\left[1+\left(\tilde{\alpha}_\lambda+\tilde{\beta}_\lambda\mathcal{A}\right)\sum_{k=1}^{\infty}(-1)^k\cos\left(2\pi k w_\lambda\right)\mathrm{e}^{-\frac{2\pi k}{\omega_{c\lambda}}|\omega_n|}\mathrm{e}^{-2\pi k|\Gamma_\lambda|}\right]. \tag{3.33}$$

I solve the equations perturbatively in the Dingle factor

$$R_{D\lambda}=\exp\left(-2\pi^2\frac{T_{D\lambda}}{\omega_{c\lambda}}\right). \tag{3.34}$$

For further calculations, I require the real part of the self-energy to first order and the imaginary part to second order in the Dingle factor, as the real and imaginary parts appear differently in the observables – only these orders are necessary to obtain Ω and σ to second order in R_D.

The equations can be solved to a sufficiently high order by a single reinsertion of the self-energy into the right-hand side of the equation for the imaginary part. Then, the right hand side can be expanded with respect to R_D, dropping terms above the first order in $\mathfrak{Re}\,\Sigma$ and above the second order in $\mathfrak{Im}\,\Sigma$. Then, the sum over Matsubara frequencies appearing in the interaction terms can be evaluated, as it takes the form of a simple geometric sum:

$$\sum_{\nu_n}\mathrm{e}^{-\frac{2\pi k}{\omega_{c\lambda}}|\nu_n|}=2\sum_{n=0}^{\infty}\mathrm{e}^{-\frac{2\pi^2 k(2n+1)}{\beta\omega_{c\lambda}}}=\frac{1}{\sinh\left(\frac{2\pi^2 k}{\beta\omega_{c\lambda}}\right)}. \tag{3.35}$$

Afterwards, the self-energy can be transformed from imaginary to real frequencies by taking $\mathrm{i}\omega_n\to\omega+\mathrm{i}\delta$ with δ being a small positive number. This procedure mixes the real and imaginary part. Then, $\epsilon_\lambda=\frac{\omega}{\omega_{c\lambda}}$ can be defined analogously to the single-band case. It is best to work with a dimensionless

self-energy $\frac{\Sigma_\lambda}{\omega_{c\lambda}}$ which takes the form

$$\begin{aligned}\frac{\mathfrak{Re}\,\Sigma_\lambda(\omega)}{\omega_{c\lambda}} =& -\tau_\lambda\left(\alpha_\lambda+\beta_\lambda\mathcal{A}\right)\sin\left[2\pi\left(\epsilon_\lambda+\frac{W_\lambda}{\omega_{c\lambda}}\right)\right]R_{D\lambda}\\ &-\frac{V_0 m_\lambda}{2\pi^2}\left(\gamma_\lambda+\delta\mathcal{A}\right)\sin\left(2\pi\frac{W_\lambda}{\omega_{c\lambda}}\right)R_{LK}\left(\frac{2\pi^2 T}{\omega_{c\lambda}}\right)R_{D\lambda}; \quad (3.36)\\ \frac{|\,\mathfrak{Im}\,\Sigma_\lambda(\omega)|}{\omega_{c\lambda}} =& \tau_\lambda\left[1-\left(\alpha_\lambda+\beta_\lambda\mathcal{A}\right)\cos\left[2\pi\left(\epsilon_\lambda+\frac{W_\lambda-\mathfrak{Re}\,\Sigma_\lambda}{\omega_{c\lambda}}\right)\right]\mathrm{e}^{-2\pi|\Gamma_\lambda|}\right.\\ &\left.+\left(\alpha_\lambda+\beta_\lambda\mathcal{A}\right)\cos\left[4\pi\left(\epsilon_\lambda+\frac{W_\lambda}{\omega_{c\lambda}}\right)\right]R_{D\lambda}^2\right], \quad (3.37)\end{aligned}$$

where $\tau_\lambda = \frac{\pi T_{D\lambda}}{\omega_{c\lambda}}$. At this point, the effect of the introduced impurities and interactions is evident. At zeroth order in R_D, the impurities lead to a constant imaginary part of the self-energy analogous to the lifetime in the single-band case Eq. (2.19). At higher orders, intraband impurity scattering proportional to α_λ introduces terms oscillating with a frequency associated with band with the same index as the self-energy in the imaginary and real parts. Intraband interactions proportional to γ_λ have the same effect, but only in the real part. Interband scattering (proportional to β_λ) and interactions (proportional to θ and η) have a more profound effect. In self-energy with index λ, there are terms oscillating with the frequency associated with band $\bar{\lambda}$. it is this feature that leads to oscillations of observables with combination frequencies.

The intraband terms will only lead to a renormalization of oscillation amplitudes in observables. They are unnecessary to obtain the desired effect, but I include them for completeness. The two types of interband interactions have the same impact when the interactions are point-like – only a single type is enough to produce combination frequencies.

3.4 Interaction-induced anomalous quantum oscillations

3.4.1 De Haas-van Alphen effect

The density of states and conductivity kernels in the multiband case are straightforwardly obtained from analogous formulas for single-band systems Eq. (2.27), Eq. (2.57) and Eq. (2.71). One needs to add a band index to all instances of, m, then change $\Gamma \to \Gamma_\lambda = \frac{\mathfrak{Im}\,\Sigma_\lambda}{\omega_{c\lambda}}$, $R_D \to \mathrm{e}^{-2\pi|\Gamma_\lambda|}$, $\mu \to W_\lambda - \mathfrak{Re}\,\Sigma_\lambda$. Then, the expression should be summed over the band index.

After these modifications, the density of states takes the form

$$\rho(\omega) = \sum_\lambda \frac{m_\lambda}{2\pi} \left(1 + 2 \sum_{k=1}^{\infty} (-1)^k \cos\left[2\pi k \left(\epsilon_\lambda + w_\lambda\right)\right] \mathrm{e}^{-2\pi k |\Gamma_\lambda|} \right). \tag{3.38}$$

Now, I use the derived self-energy Eq. (3.36), Eq. (3.37) and expand ρ to second order in the Dingle factor $R_{D\lambda}$. Due to the self-energy with index λ oscillating with frequencies associated with band $\bar{\lambda}$, terms mixing the two bands appear. They can be simplified using

$$\sin(a)\sin(b) = \frac{1}{2}\left[\cos(a-b) - \cos(a+b)\right], \tag{3.39}$$

to leave only one cosine in each term. Keeping only oscillating terms up to second order in R_D, the density of states takes the form

$$\begin{aligned}
\rho(E) = &- \sum_\lambda \frac{m_\lambda}{\pi} \cos\left[2\pi \frac{E + W_\lambda}{\omega_{c\lambda}}\right] R_{D\lambda} \\
&+ \sum_\lambda \frac{m_\lambda}{\pi} \left(1 - 2\pi\tilde{\alpha}_\lambda \tau_\lambda\right) \cos\left[4\pi \frac{E + W_\lambda}{\omega_{c\lambda}}\right] R_{D\lambda}^2 \\
&- \sum_\lambda \frac{V_0 m_\lambda^2 \gamma_\lambda}{2\pi^2} \cos\left[2\pi \frac{E + 2W_\lambda}{\omega_{c\lambda}}\right] R_{LK}\left(\frac{2\pi^2 T}{\omega_{c\lambda}}\right) R_{D\lambda}^2 \\
&- 2\sum_\lambda \tilde{\beta}_\lambda m_\lambda \tau_\lambda \cos\left[2\pi \frac{E + W_+}{\omega_+}\right] R_{D1} R_{D2} \\
&- \sum_\lambda \frac{V_0 m_\lambda^2 \delta}{2\pi^2} \cos\left[2\pi \left(\frac{E}{\omega_{c\lambda}} + \frac{W_+}{\omega_+}\right)\right] R_{LK}\left(\frac{2\pi^2 T}{\omega_{c\bar{\lambda}}}\right) R_{D1} R_{D2} \\
&+ \sum_\lambda \frac{V_0 m_\lambda^2 \delta}{2\pi^2} \cos\left[2\pi \left(\frac{E}{\omega_{c\lambda}} + \frac{W_-}{\omega_-}\right)\right] R_{LK}\left(\frac{2\pi^2 T}{\omega_{c\bar{\lambda}}}\right) R_{D1} R_{D2},
\end{aligned} \tag{3.40}$$

where $\omega_\pm^{-1} = \omega_{c1}^{-1} \pm \omega_{c2}^{-1}$ and $\frac{W_\pm}{\omega_\pm} = \frac{W_1}{\omega_{c1}} \pm \frac{W_2}{\omega_{c2}}$. At this point, the impact of introduced impurities and interactions becomes evident. At first order in R_D, they play no role and the oscillations have the same form as in the single-band case Eq. (2.27). At second order, there are three kinds of second harmonic terms. In the second line, there is one present in the single-band case and one induced by intraband impurity scattering. In the third line, one sees a second harmonic term induced by intraband interactions. It is unusual, because it already appears with a temperature damping R_{LK}. In the fourth line, there appears a sum frequency term induced by interband

impurity scattering. Finally in the fourth and fifth line, one finds sum and difference frequency terms induced by interband interactions – once again, they are proportional to the Lifshitz-Kosevich temperature damping. The appearance of the temperature damped difference frequency in the density of states is one of the key results of this work.

To obtain the thermodynamic potential, I need to first integrate ρ over energy to get $N(E)$ Eq. (2.30). The integrals are of the form

$$\int_{-\infty}^{\mu} dE \cos\left(2\pi\frac{E}{\omega_c}\right) = \frac{\omega_c}{2\pi}\sin\left(2\pi\frac{\mu}{\omega_c}\right). \tag{3.41}$$

Their effect is to add a prefactor (the inverse of the quantity multiplying E in the cosine) After that, N needs to be integrated with the Fermi-Dirac distribution like in Eq. (2.29). As indicated by Eq. (2.32), this effectively means setting E to 0 and adding a factor $\frac{\pi T}{\sinh(a\pi T)}$ (which can be absorbed into R_{LK}), where a is the prefactor of E inside of the sine, and changing the phase from sine to cosine. After these steps, the thermodynamic potential turns out to equal

$$\begin{aligned}
\Omega = &\sum_{\lambda} A_{\lambda}^{(1)} R_{LK}\left(\frac{2\pi^2 T}{\omega_{c\lambda}}\right)\cos\left(2\pi\frac{W_\lambda}{\omega_{c\lambda}}\right) R_{D\lambda} \\
&+ \sum_{\lambda}\left[A_{\lambda}^{(2)} R_{LK}\left(\frac{4\pi^2 T}{\omega_{c\lambda}}\right) + B_{\lambda}^{(2)} R_{LK}\left(\frac{2\pi^2 T}{\omega_{c\lambda}}\right)^2\right]\cos\left(4\pi\frac{W_\lambda}{\omega_{c\lambda}}\right) R_{D\lambda}^2 \\
&+ A_{+} R_{LK}\left(\frac{2\pi^2 T}{\omega_{+}}\right)\cos\left(2\pi\frac{W_+}{\omega_+}\right) R_{D1}R_{D2} \\
&+ B_{+} R_{LK}\left(\frac{2\pi^2 T}{\omega_{c1}}\right) R_{LK}\left(\frac{2\pi^2 T}{\omega_{c2}}\right)\cos\left(2\pi\frac{W_+}{\omega_+}\right) R_{D1}R_{D2} \\
&+ B_{-} R_{LK}\left(\frac{2\pi^2 T}{\omega_{c1}}\right) R_{LK}\left(\frac{2\pi^2 T}{\omega_{c2}}\right)\cos\left(2\pi\frac{W_-}{\omega_-}\right) R_{D1}R_{D2}
\end{aligned} \tag{3.42}$$

with the lengthy amplitudes given in appendix B.

The derived thermodynamic potential has interesting features arising due to interband interactions. Most importantly, two new oscillation frequencies appear – the difference and sum frequency. There are two types of temperature dependencies of the second harmonic and sum frequency terms: the ones produced by impurity scattering decay with a single Lifshitz-Kosevich factor with ω_+ (i.e. the sum of the effective masses) in the argument, and the ones coming from interactions decay with two LK factors with effective masses of both bands in the argument. The difference frequency term appears only with the second kind of temperature damping. The main result of

this section is that difference frequency oscillations appear in thermodynamic quantities solely due to the inclusion of electronic interactions between bands (as indicated by the amplitude B_- being proportional to interband interaction strength δ).

3.4.2 Shubnikov-de Haas effect

The computation of the longitudinal and transversal conductivity for the two-band system follows similar steps to the above calculation of the thermodynamic potential. First, I obtain the formulas for the conductivity kernels by modifying Eq. (2.57) and Eq. (2.71)

$$\hat{\sigma}_{xx}(\omega) = \sigma_0 \sum_\lambda \frac{(\epsilon_\lambda + w_\lambda)|\Gamma_\lambda|}{1+4\Gamma_\lambda^2}\left[1 + 2\sum_{k=1}^{\infty}(-1)^k \cos[2\pi k(\epsilon_\lambda + w_\lambda)] R_{D\lambda}^k\right]; \tag{3.43}$$

$$\hat{\sigma}_{xy}(\omega) = -\frac{\sigma_0}{2} \sum_\lambda \frac{(\epsilon_\lambda + w_\lambda)}{1+4\Gamma_\lambda^2}\left[1 + (3+4\Gamma_\lambda^2)\sum_{k=1}^{\infty}(-1)^k \cos[2\pi k(\epsilon_\lambda + w_\lambda)] R_{D\lambda}^k\right]. \tag{3.44}$$

Then, I expand the kernels with respect to the Dingle factor R_D, keeping terms to the second order. In this case, I need second-order terms from $\mathfrak{Im}\,\Sigma_\lambda$, as they will contribute through the non-oscillating part of the kernel. Once again, I obtain terms oscillating with the combination frequencies. I integrate the kernels with the derivative of the Fermi-Dirac distribution as in Eq. (2.51) to obtain the final form of the longitudinal conductivity

$$\begin{aligned}
\frac{\sigma_{xx}}{\sigma_0} =& \sum_\lambda C_{xx,\lambda}^{(1)} R_{LK}\left(\frac{2\pi^2 T}{\omega_{c\lambda}}\right)\cos\left(2\pi\frac{W_\lambda}{\omega_{c\lambda}}\right) R_{D\lambda} \\
&+ \sum_\lambda \left[C_{xx,\lambda}^{(2)} R_{LK}\left(\frac{4\pi^2 T}{\omega_{c\lambda}}\right) + D_{xx,\lambda}^{(2)} R_{LK}\left(\frac{2\pi^2 T}{\omega_{c\lambda}}\right)^2\right]\cos\left(4\pi\frac{W_\lambda}{\omega_{c\lambda}}\right) R_{D\lambda}^2 \\
&+ C_{xx,+} R_{LK}\left(\frac{2\pi^2 T}{\omega_{+}}\right)\cos\left(2\pi\frac{W_+}{\omega_{+}}\right) R_{D1} R_{D2} \\
&+ D_{xx,+} R_{LK}\left(\frac{2\pi^2 T}{\omega_{c1}}\right) R_{LK}\left(\frac{2\pi^2 T}{\omega_{c2}}\right)\cos\left(2\pi\frac{W_+}{\omega_{+}}\right) R_{D1} R_{D2} \\
&+ C_{xx,-} R_{LK}\left(\frac{2\pi^2 T}{\omega_{-}}\right)\cos\left(2\pi\frac{W_-}{\omega_{-}}\right) R_{D1} R_{D2} \\
&+ D_{xx,-} R_{LK}\left(\frac{2\pi^2 T}{\omega_{c1}}\right) R_{LK}\left(\frac{2\pi^2 T}{\omega_{c2}}\right)\cos\left(2\pi\frac{W_-}{\omega_{-}}\right) R_{D1} R_{D2},
\end{aligned} \tag{3.45}$$

and the form of σ_{xy} is the same, only with different amplitudes C_{xy}, D_{xy}. For explicit forms of the amplitudes, see appendix B.

In the conductivities, the second-order terms appear with two types of temperature dependencies. The second harmonic has a part decaying with a single LK factor with the same argument as the first harmonic multiplied by 2, and another which decays with a square of the first harmonic LK factor. The sum frequency has a part produced by impurities which is proportional to the LK factor with the sum of two effective masses in the argument and a second one produced by interactions that is proportional to a product of two LK factors with different masses. The difference frequency term is of most interest, as the impurity-induced part is proportional to a LK factor with a difference of effective masses in the argument, and thus decays with increasing temperature much slower than the interaction-induced one. it is a key result of this work – the combination of the two mechanisms will lead to an anomalous temperature dependence of the difference frequency discussed in section 3.5.

3.4.3 Extension to three dimensions

The results of previous sections are straightforwardly generalized to three dimensions as shown in [18]. In this case, the dispersion becomes dependent on the momentum parallel to the magnetic field k_z and takes the form

$$\varepsilon_{l,k_z,\lambda} = \omega_{c\lambda}\left(l+\frac{1}{2}\right) + \frac{k_z^2}{2m_\lambda} - W_\lambda. \tag{3.46}$$

To transform the equations to their three-dimensional form, it is enough to take $W_\lambda \to \frac{k_z^2}{2m_\lambda}$ and add a sum $\frac{1}{L_z}$ in the self-energy, density of states and conductivity. In each case, it will result in an integral of the type

$$\int_{-\infty}^{\infty} dx \left(\mu - x^2\right)^n \mathrm{e}^{\pm 2\pi \mathrm{i}\left(\mu - x^2\right)} = \frac{\mu^n}{\sqrt{2}} \mathrm{e}^{\pm 2\pi \mathrm{i}\mu \mp \mathrm{i}\frac{\pi}{4}}, \tag{3.47}$$

solved in appendix A. As a consequence, the magnetization and conductivity oscillations differ from those in Eq. (2.34), Eq. (2.59) and Eq. (2.72) only by a phase ($\frac{\pi}{4}$ in first and second harmonics, $\frac{\pi}{2}$ in sum and 0 in difference frequency) and the modified amplitudes. As an example, the oscillatory part

of the longitudinal conductivity in 3D is

$$\begin{aligned}\frac{\sigma_{xx}^{(3D)}}{\sigma_0} =& \sum_\lambda C'^{(1)}_{xx,\lambda} R_{LK}\left(\frac{2\pi^2 T}{\omega_{c\lambda}}\right)\cos\left(2\pi\frac{W_\lambda}{\omega_{c\lambda}}-\frac{\pi}{4}\right)R_{D\lambda} \\ &+\sum_\lambda C'^{(2)}_{xx,\lambda} R_{LK}\left(\frac{4\pi^2 T}{\omega_{c\lambda}}\right)\cos\left(4\pi\frac{W_\lambda}{\omega_{c\lambda}}-\frac{\pi}{4}\right)R^2_{D\lambda} \\ &+\sum_\lambda D'^{(2)}_{xx,\lambda} R_{LK}\left(\frac{2\pi^2 T}{\omega_{c\lambda}}\right)^2\cos\left(4\pi\frac{W_\lambda}{\omega_{c\lambda}}-\frac{\pi}{4}\right)R^2_{D\lambda} \\ &+C'_{xx,+} R_{LK}\left(\frac{2\pi^2 T}{\omega_{+}}\right)\cos\left(2\pi\frac{W_+}{\omega_{+}}-\frac{\pi}{2}\right)R_{D1}R_{D2} \\ &+D'_{xx,+} R_{LK}\left(\frac{2\pi^2 T}{\omega_{c1}}\right)R_{LK}\left(\frac{2\pi^2 T}{\omega_{c2}}\right)\cos\left(2\pi\frac{W_+}{\omega_{+}}-\frac{\pi}{2}\right)R_{D1}R_{D2} \\ &+C'_{xx,-} R_{LK}\left(\frac{2\pi^2 T}{\omega_{-}}\right)\cos\left(2\pi\frac{W_-}{\omega_{-}}\right)R_{D1}R_{D2} \\ &+D'_{xx,-} R_{LK}\left(\frac{2\pi^2 T}{\omega_{c1}}\right)R_{LK}\left(\frac{2\pi^2 T}{\omega_{c2}}\right)\cos\left(2\pi\frac{W_-}{\omega_{-}}\right)R_{D1}R_{D2}. \quad (3.48)\end{aligned}$$

The transversal conductivity and the magnetization oscillations change in the same way.

3.5 Experimental consequences

3.5.1 General remarks

Oscillations of magnetization and conductivity as a function of $\frac{1}{B}$ derived in previous sections can, in principle, be directly observed. By measuring the observables for various magnitudes of the external magnetic field, and then taking the Fourier transform, one can get the frequencies by determining the position of the peaks. The temperature dependence is obtained by repeating the measurement at different temperatures and then finding either the oscillation amplitude at some value of B or the height of the Fourier peaks as a function of temperature.

My model of interband interaction-induced combination frequencies has a single experimental signature: additional contributions to the second harmonic, sum and difference frequency, which depend on temperature through R^2_{LK}. They appear in both thermodynamical and transport quantities. In second harmonic and sum frequency terms, this modification is likely hard

to observe. The reason is that

$$R_{LK}\left(\frac{2\pi^2 T}{\omega_+}\right) \approx R_{LK}\left(\frac{2\pi^2 T}{\omega_{c1}}\right) R_{LK}\left(\frac{2\pi^2 T}{\omega_{c2}}\right), \tag{3.49}$$

as illustrated in figure 3.1.

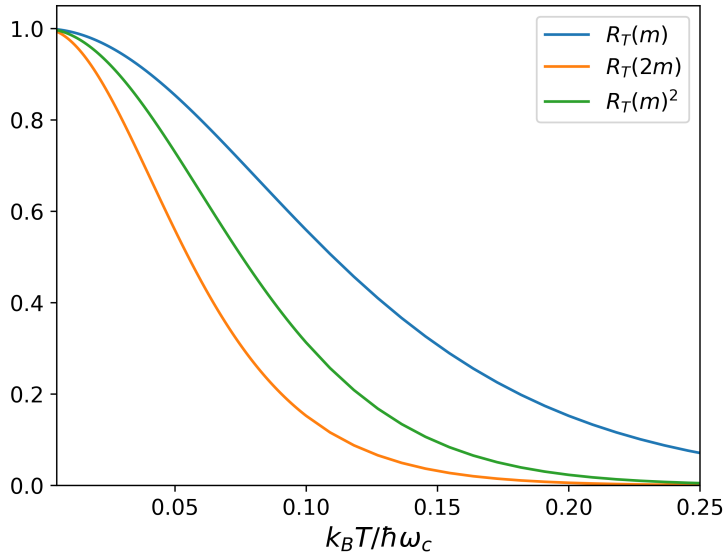

Figure 3.1: Comparison of the temperature dependencies of the sum frequency for induced by impurities (in orange) and interactions (in green) and the temperature dependence of the first harmonic (in blue). The effective masses of electrons in both bands are taken to be the same. Notation $R_T(m) = R_{LK}(\frac{2\pi^2 k_B T}{\hbar\omega_c})$ was introduced for simplicity.

A more promising prospect is observing a difference frequency at low temperatures in thermodynamics, which appears only due to interactions and is not present in a model with just impurities. A low-temperature difference frequency has been discovered in magnetization in some materials, which I discuss in section 3.5.2. It can be argued that it is produced by electronic interactions, however, there are other mechanisms leading to the same effect, like magnetic interaction [22] (discussed in appendix D).

The strongest possibility of experimental verification of my model is given by the difference frequency in conductivity. The difference frequency terms

take the form

$$\frac{\sigma^{-}_{xx}}{\sigma_0} = \left[C_{xx,-} R_{LK}\left(\frac{2\pi^2 T}{\omega_-}\right) + D_{xx,-} R_{LK}\left(\frac{2\pi^2 T}{\omega_{c1}}\right) R_{LK}\left(\frac{2\pi^2 T}{\omega_{c2}}\right)\right] \times \cos\left(2\pi \frac{W_-}{\omega_-}\right) R_{D1} R_{D2}; \tag{3.50}$$

$$\frac{\sigma^{-}_{xy}}{\sigma_0} = \left[C_{xy,-} R_{LK}\left(\frac{2\pi^2 T}{\omega_-}\right) + D_{xy,-} R_{LK}\left(\frac{2\pi^2 T}{\omega_{c1}}\right) R_{LK}\left(\frac{2\pi^2 T}{\omega_{c2}}\right)\right] \times \cos\left(2\pi \frac{W_-}{\omega_-}\right) R_{D1} R_{D2}. \tag{3.51}$$

Here, the contribution induced by impurities is damped by $R_{LK}\left(\frac{2\pi^2 T}{\omega_-}\right)$, which decays very slowly with temperature provided $m_1 \approx m_2$. In contrast, the interaction-induced contribution decays quickly due to the R^2_{LK} temperature dependence. The combination of both effects produces an anomalous, non-Lifshitz-Kosevich temperature dependence of the amplitude, with a part that survives to high temperature and an additional change introduced at low temperature. The shape of the temperature dependence is governed by the ratio of amplitudes $\frac{D_-}{C_-}$. As illustrated in figure 3.2, depending on the relative sign and magnitude of the amplitudes, a wide array of shapes is possible.

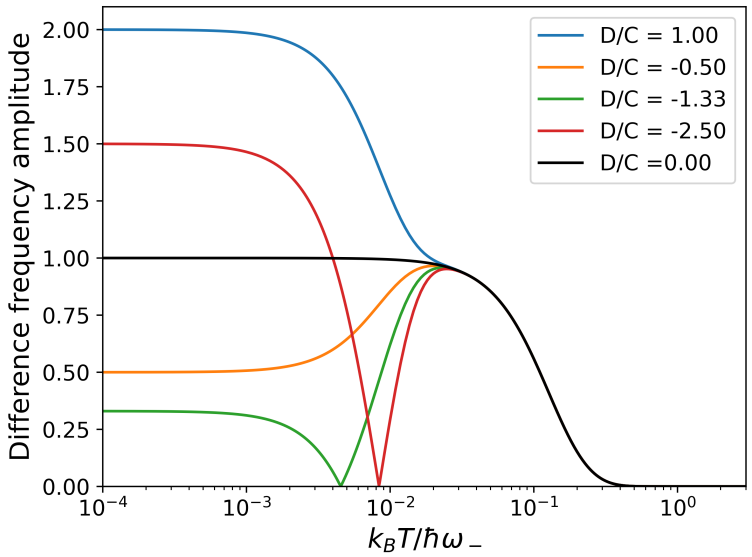

Figure 3.2: Temperature dependencies of the difference frequency given by the derived model for different values of the ratio of amplitudes of the impurity- and interaction-induced parts. For visualization purposes, $m_1 = m_e$ and $m_2 = 1.1m_e$ were chosen.

It should be noted that the amplitudes C_-, D_- appearing in the derived model (written explicitly in appendix B) are polynomial functions of the magnetic field and can even change sign at some values of the field. Even though the amplitudes vary much slower than the oscillatory factor, they could influence the measured temperature dependence if it is determined through the height of the Fourier transform peak. Due to the dependence of amplitudes on a multitude of material-dependent parameters (effective masses m_λ, energy shifts W_λ, Dingle temperatures $T_{D\lambda}$, impurity and interaction parameters α_λ, β_λ, γ_λ, δ), I investigate the resulting temperature dependence only in the case of a particular material in section 3.5.2.

Thanks to the derived model, one can obtain information about the role of interactions and impurities in a material. The dimensionless parameters α_λ, β_λ, γ_λ, δ can provide insight into the relative strength of inter- and intraband impurity scattering and interaction effects. By fitting the obtained formulas to experimental data (as in the following section 3.5.2), one can determine these parameters through a measurement of the temperature dependence of combination frequency quantum oscillations.

3.5.2 Relation to experimental data

Resistivity measurement in CoSi

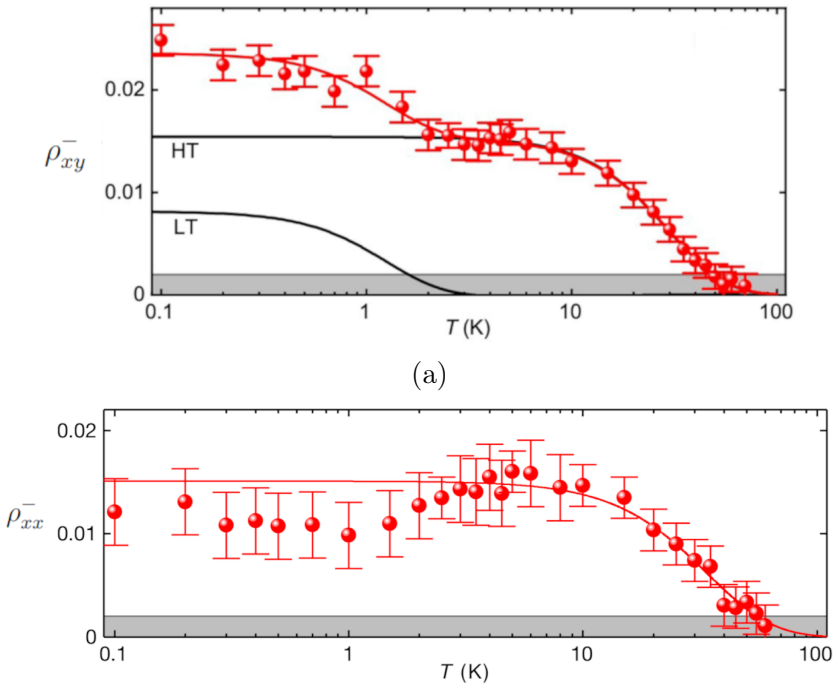

Figure 3.3: Temperature dependencies of the difference frequency amplitude in longitudinal (a) (transversal (b)) resistivities measured in CoSi, reproduced with permission from [9]. Note that at low temperatures, the amplitude slightly decreases in longitudinal resistivity and noticeably increases in transversal resistivity.

In a resistivity measurement in CoSi [9], the temperature dependencies of the difference frequency term depicted in figure 3.3 were observed. One can see that in longitudinal resistivity the amplitude slightly drops at low temperature (within the margin of error), while in transversal resistivity, the amplitude grows noticeably at low temperature. Here, I fit the derived model to the data obtained in the experiment. One difficulty is that in this work I calculated conductivities, while the measurement concerns resistivities. In

the case $\sigma_{xx} = \sigma_{yy}$, $\sigma_{xy} = -\sigma_{yx}$ they are related like

$$\rho_{xx} = \frac{\sigma_{xx}}{\sigma_{xx}^2 + \sigma_{xy}^2}; \tag{3.52}$$

$$\rho_{xy} = -\frac{\sigma_{xy}}{\sigma_{xx}^2 + \sigma_{xy}^2}. \tag{3.53}$$

It seems that the oscillations of longitudinal/transversal resistivity are produced by a mix of oscillations of both conductivities. To further investigate this, I split the conductivities as

$$\sigma_{\alpha\beta} = \sigma_{\alpha\beta}^{(0)} + \tilde{\sigma}_{\alpha\beta}, \tag{3.54}$$

where $\sigma_{\alpha\beta}^{(0)}$ is the non-oscillating part of the conductivity and $\tilde{\sigma}_{\alpha\beta}(B)$ is the oscillatory part with $\tilde{\sigma}_{\alpha\beta}/\sigma_{\alpha\beta}^{(0)} \ll 1$.

When I expand Eq. (3.52) and Eq. (3.53) to first order with respect to $\frac{\tilde{\sigma}_{xx}}{\sigma_{xx}^{(0)}}$ and $\frac{\tilde{\sigma}_{xy}}{\sigma_{xy}^{(0)}}$, I obtain

$$\begin{aligned}\rho_{xx} =& \frac{\sigma_{xx}^{(0)}}{\left(\sigma_{xx}^{(0)}\right)^2 + \left(\sigma_{xy}^{(0)}\right)^2} - \frac{\left(\sigma_{xx}^{(0)}\right)^2 - \left(\sigma_{xy}^{(0)}\right)^2}{\left(\left(\sigma_{xx}^{(0)}\right)^2 + \left(\sigma_{xy}^{(0)}\right)^2\right)^2}\tilde{\sigma}_{xx} \\ & - \frac{2\sigma_{xx}^{(0)}\sigma_{xy}^{(0)}}{\left(\left(\sigma_{xx}^{(0)}\right)^2 + \left(\sigma_{xy}^{(0)}\right)^2\right)^2}\tilde{\sigma}_{xy};\end{aligned} \tag{3.55}$$

$$\begin{aligned}\rho_{xy} =& -\frac{\sigma_{xy}^{(0)}}{\left(\sigma_{xx}^{(0)}\right)^2 + \left(\sigma_{xy}^{(0)}\right)^2} + \frac{2\sigma_{xx}^{(0)}\sigma_{xy}^{(0)}}{\left(\left(\sigma_{xx}^{(0)}\right)^2 + \left(\sigma_{xy}^{(0)}\right)^2\right)^2}\tilde{\sigma}_{xx} \\ & - \frac{\left(\sigma_{xx}^{(0)}\right)^2 - \left(\sigma_{xy}^{(0)}\right)^2}{\left(\left(\sigma_{xx}^{(0)}\right)^2 + \left(\sigma_{xy}^{(0)}\right)^2\right)^2}\tilde{\sigma}_{xy}.\end{aligned} \tag{3.56}$$

I notice that the oscillating part of the longitudinal/transversal resistivity are a combination of the oscillating parts of both conductivities. Since the prefactors depend on the magnetic field through $\sigma_{xx}^{(0)}$ and $\sigma_{xy}^{(0)}$, they introduce an unknown magnetic field dependence to the quantum oscillation amplitudes. This makes the connection between my model and the CoSi measurement challenging. To mitigate this, a different experimental technique is required. If the temperature dependence of the difference frequency amplitude is measured for a single value of the magnetic field, the magnetic field dependence

of the amplitude becomes irrelevant. Alternatively, the full resistivities obtained in a measurement similar to the one in CoSi could be used to compute the full conductivities before the Fourier analysis, sidestepping the problem entirely.

For simplicity, in this work I ignore the magnetic field dependence of the amplitude introduced by the conversion from conductivities to resistivities – I set $\sigma_{xx}^{(0)}$ and $\sigma_{xy}^{(0)}$ to constants. Their only effect will be to introduce a relative magnitude difference between the longitudinal and transversal resistivity oscillations called κ. I will preform a fit to the following formulas for the difference frequency oscillations of resistivity:

$$\begin{aligned}\frac{\sigma_{xx}^{-}}{\sigma_0} =&\kappa\left[C_{xx,-}R_{LK}\left(\frac{2\pi^2T}{\omega_-}\right)+D_{xx,-}R_{LK}\left(\frac{2\pi^2T}{\omega_{c1}}\right)R_{LK}\left(\frac{2\pi^2T}{\omega_{c2}}\right)\right]\\&\times\cos\left(2\pi\frac{W_-}{\omega_-}\right)R_{D1}R_{D2};\end{aligned}\tag{3.57}$$

$$\begin{aligned}\frac{\sigma_{xy}^{-}}{\sigma_0} =&\left[C_{xy,-}R_{LK}\left(\frac{2\pi^2T}{\omega_-}\right)+D_{xy,-}R_{LK}\left(\frac{2\pi^2T}{\omega_{c1}}\right)R_{LK}\left(\frac{2\pi^2T}{\omega_{c2}}\right)\right]\\&\times\cos\left(2\pi\frac{W_-}{\omega_-}\right)R_{D1}R_{D2}.\end{aligned}\tag{3.58}$$

In [9], the height of the Fourier peak was used to determine the temperature dependence of the difference frequency. To compute the difference frequency amplitude at a given temperature predicted by my model, I generate values of σ_{xx}^{-} and σ_{xy}^{-} (as in Eq. (3.50) and Eq. (3.51) with field-dependent amplitudes as in appendix B) for values of $B \in$ [7 T, 20 T]. I perform a discrete Fourier transform with respect to $\frac{1}{B}$. I use zero-padding to smooth out the results and a Hamming window to mitigate the effects of taking a finite interval. Then, I fit a Gaussian to the peak to extract the height of the peak.

In the fit, I use numerical values of $F_\lambda = \frac{2\pi W_\lambda m_\lambda}{\hbar e}$ ($F_1 = 565$ T, $F_2 = 663$ T), m_λ ($m_1 = 0.92m_e$, $m_2 = 0.92m_e$) and $T_{D\lambda}$ ($T_{D1} = 1.3$ K, $T_{D2} = 1.2$ K), which enters through $\tau_\lambda = \frac{\pi k_B T_{D\lambda} m_\lambda}{\hbar e B}$ in amplitudes C, D, measured in [9]. I set $V_0 = \frac{1}{m_e}$ for dimensional reasons – the particular value doesn't matter, as it always appears together with the fitting parameter δ. The values of α_λ, β and δ remain undetermined. I restrict the first two to be positive, but I allow $\delta = \eta - \theta$ to take any real value.

I fitted Eq. (3.57) and Eq. (3.58) to longitudinal and transversal resistivity data simultaneously. I obtained $\kappa = 3.8 \pm 0.2$, $\alpha_1 = 3 \pm 2$, $\alpha_2 = 1.9 \pm 0.7$, $\beta = (3.9 \pm 0.3) \times 10^{-4}$, $\delta = (-2.4 \pm 0.1) \times 10^{-4}$. The temperature dependencies for this choice of parameters together with the data points are plotted in figures 3.4 and 3.5.

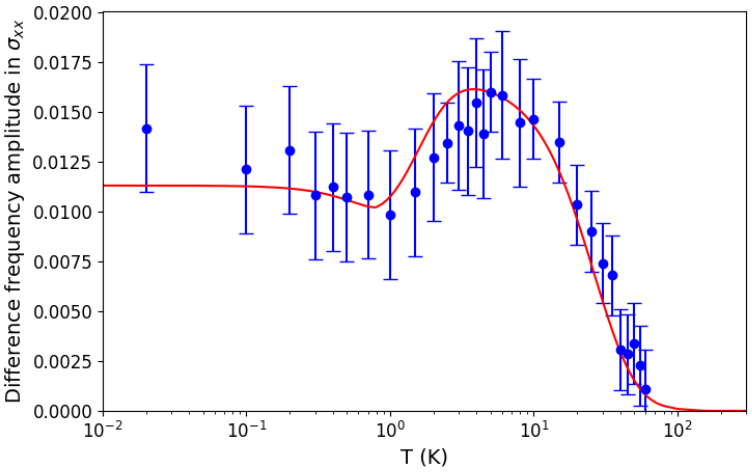

Figure 3.4: The amplitude of the difference frequency in ρ_{xx} as a function of temperature measured in CoSi (blue points with errorbars) and a fitted curve produced by the derived model (red).

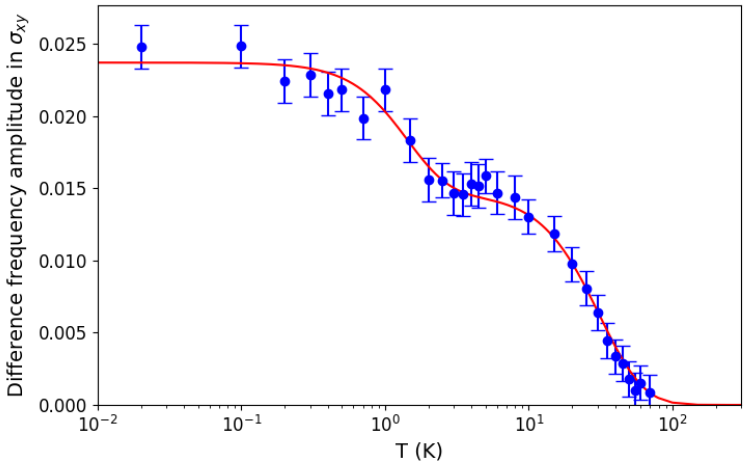

Figure 3.5: The amplitude of the difference frequency in ρ_{xy} as a function of temperature measured in CoSi (blue points with errorbars) and a fitted curve produced by the derived model (red).

The fitted curves are in excellent agreement with the data. It's worth noting that the temperature dependence in longitudinal conductivity couldn't be obtained if the amplitudes C_-, D_- were taken to be constant like in figure 3.2. The appearance of a local minimum and a local maximum for non-zero temperatures is only possible because in the model the amplitudes change noticeably in the magnetic field range spanned by the measurement.

Magnetization measurements in UPd_2Al_3 and $PtCoO_2$

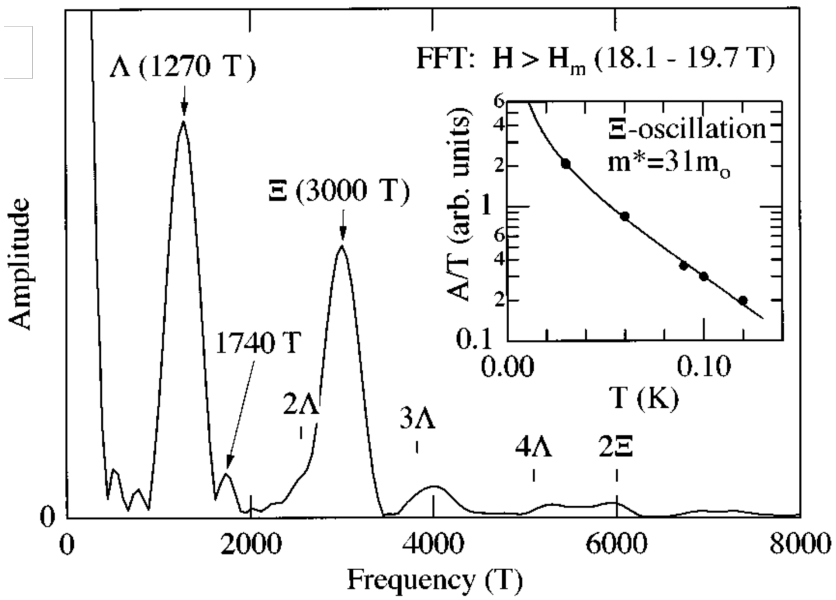

Figure 3.6: The quantum oscillation spectrum observed in a magnetization measurement in UPd_2Al_3, reproduced from [14].

A difference frequency in thermodynamics has been observed in several materials. A magnetization measurement in UPd_2Al_3 [14] resulted in a quantum oscillation spectrum in figure 3.6. One can see two fundamental frequency peaks labeled Λ and Ξ, as well as a small peak at 1740T $\approx \Xi - \Lambda$. The temperature dependence of this frequency was not measured. However, the fact that the peak is of the same magnitude as 2Λ suggests that it is also a second order effect.

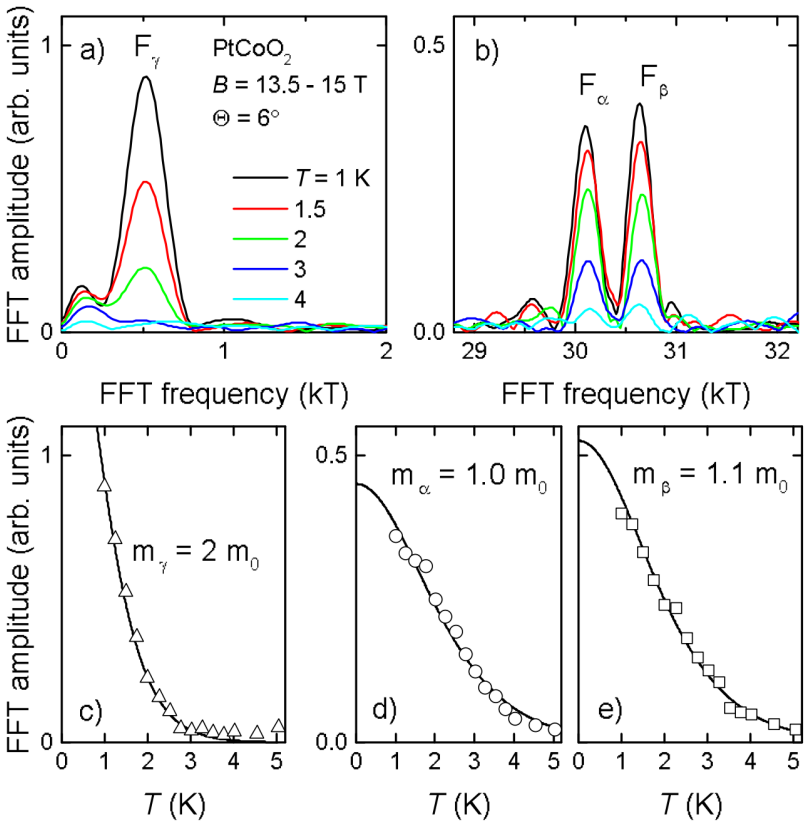

Figure 3.7: The quantum oscillation spectrum observed in a magnetization measurement in $PtCoO_2$, together with the temperature dependence of the three observed frequencies. Reproduced from [16].

A measurement of magnetization in $PtCoO_2$ resulted in a quantum oscillation spectrum in figure 3.7. The measurement was performed for different orientations of the magnetic field, resulting in different values of the fundamental frequencies F_α and F_β, but also a third frequency fulfilling $F_\gamma = F_\alpha - F_\beta$. The temperature dependence of the three frequencies was measured for a particular angle, resulting in the plots in figure 3.7. The measured effective masses fulfill $m_\gamma \approx m_\alpha + m_\beta$, which is consistent with my prediction that the temperature dependence of the difference frequency in thermodynamics is $R_{LK}\left(\frac{2\pi^2 T}{\omega_{c1}}\right) R_{LK}\left(\frac{2\pi^2 T}{\omega_{c2}}\right) \approx R_{LK}\left(\frac{2\pi^2 T}{\omega_+}\right)$.

Chapter 4

Conclusion

The standard Lifshitz-Kosevich theory of quantum oscillations has proven to be incredibly reliable for the 70 years since its invention. The improvement of experimental techniques in the recent years has brought new insights, revealing the role of interactions in generating oscillations which do not appear in the LK theory. In this work, I derived a mechanism for the appearance of non-Onsager frequencies in multiband systems due to interactions between electrons in different bands.

A proper treatment of impurity scattering and electronic interactions in the Landau level basis reveals oscillations of the self-energy as a function of the magnetic field. In the case of impurities, the second-order contribution gives oscillations of the real and imaginary parts of the self energy that differ only by a $\frac{\pi}{2}$ phase. In multiband systems with interband impurity scattering, this leads to temperature stable difference frequency oscillations in conductivity. Interactions have a similar effect, but with two crucial disparities. The lowest-order diagrams are purely real and they contain a temperature damping term. This results in a difference frequency in both thermodynamics and conductivity, which, in contrast to the impurity-induced one, is strongly temperature damped.

The combination of impurities and interactions leads to a novel type of temperature dependence. When including both effects, the amplitude of the difference frequency is comprised of a low temperature and a high temperature part, which can be additive or subtractive. This possibly explains the temperature dependence observed in resistivity measurements in CoSi.

The model developed in this thesis could be expanded in multiple directions. The case of extended impurities or Coulomb interactions described in appendix C could be investigated further, possibly with numerical methods. Higher order diagrams could introduce new effects as well. Finally, finding additional experimental signatures of the model would strengthen its connec-

tion to data and make it possible to distinguish between it and other models giving similar predictions.

In conclusion, interband electronic interactions can significantly influence the quantum oscillation spectrum. They lead to the appearance of frequencies beyond Lifshitz-Kosevich theory with a novel temperature dependence.

Appendix A

Integral formulas

In this appendix, I prove formulas used in the work.

A.1 Poisson resummation

The Poisson summation formula states that

$$\sum_{n=0}^{\infty} f(n) = \sum_{k=-\infty}^{\infty} \int_0^{\infty} dx\, \mathrm{e}^{2\pi \mathrm{i} k x} f(x). \tag{A.1}$$

It becomes evident after realizing that

$$\sum_{n=-\infty}^{\infty} \delta\left(x+n\right) = \sum_{k=-\infty}^{\infty} \mathrm{e}^{2\pi \mathrm{i} k x}, \tag{A.2}$$

as after multiplying by $f(x)$ and integrating both sides with respect to x one obtains Eq. (A.1).

A.2 Temperature convolution

The integral required to compute the temperature dependence of quantum oscillations is

$$\begin{aligned}
\int_{-\infty}^{\infty} dx \frac{\mathrm{e}^{\mathrm{i}\alpha x}}{1+\mathrm{e}^{x}} &= 2\pi \mathrm{i} \left[\theta(\alpha) \sum_{k=0}^{\infty} \mathrm{Res}_{\mathrm{i}\pi(2k+1)} - \theta(-\alpha) \sum_{k=-1}^{-\infty} \mathrm{Res}_{\mathrm{i}\pi(2k+1)} \right] \frac{\mathrm{e}^{\mathrm{i}\alpha x}}{1+\mathrm{e}^{x}} \\
&= -2\pi \mathrm{i} \mathrm{e}^{-\pi\alpha} \left[\theta(\alpha) \sum_{k=0}^{\infty} \mathrm{e}^{-2\pi k \alpha} - \theta(-\alpha) \sum_{k=1}^{\infty} \mathrm{e}^{2\pi k \alpha} \right] \\
&= \frac{-\mathrm{i}\pi}{\sinh(\pi\alpha)}.
\end{aligned} \tag{A.3}$$

A.3 Oscillator eigenfunction integral

The integral of $\mathrm{e}^{\mathrm{i}q_y y}$ with the harmonic oscillator eigenfunctions used in the Feynman rules is

$$\begin{aligned}
\mathcal{I}\left(k_x,\mathbf{q},l,l'\right) =& \int dy\, \mathrm{e}^{\mathrm{i}q_y y}\psi^*_{l'}\left(y-\frac{k_x+q_x}{eB}\right)\psi_l\left(y-\frac{k_x}{eB}\right)\\
=&\frac{\mathrm{e}^{\frac{\mathrm{i}q_y k_x}{eB}}}{\sqrt{2^{l+l'}l!l'!}}\sqrt{\frac{eB}{\pi}}\int dy\, \mathrm{e}^{-\frac{eB}{2}y^2-\frac{eB}{2}(y-\frac{q_x}{eB})^2+\mathrm{i}q_y y}\\
&H_{l'}\left(\sqrt{eB}(y-\frac{q_x}{eB})\right)H_l\left(\sqrt{eB}y\right)\\
=&\frac{\mathrm{e}^{\frac{\mathrm{i}q_y(2k_x+q_x)}{2eB}}\mathrm{e}^{-\frac{\mathbf{q}^2}{2eB}}}{\sqrt{2^{l+l'}l!l'!\pi}}\int dy\, \mathrm{e}^{-y^2}H_{l'}\left(y+\frac{-q_x+\mathrm{i}q_y}{2\sqrt{eB}}\right)H_l\left(y+\frac{q_x+iq_y}{2\sqrt{eB}}\right)\\
=&\begin{cases}\sqrt{\frac{l!}{l'!}}\left(\frac{-q_x+iq_y}{\sqrt{2eB}}\right)^{l'-l}\mathrm{e}^{\mathrm{i}q_y\frac{q_x+2k_x}{2eB}}\mathrm{e}^{-\frac{\mathbf{q}^2}{4eB}}L_l^{l'-l}\left(\frac{\mathbf{q}^2}{2eB}\right) & l\le l'\\ \sqrt{\frac{l'!}{l!}}\left(\frac{q_x+iq_y}{\sqrt{2eB}}\right)^{l-l'}\mathrm{e}^{\mathrm{i}q_y\frac{q_x+2k_x}{2eB}}\mathrm{e}^{-\frac{\mathbf{q}^2}{4eB}}L_{l'}^{l-l'}\left(\frac{\mathbf{q}^2}{2eB}\right) & l'<l\end{cases}\\
=&\sqrt{\frac{l!}{l'!}}\left(\frac{-q_x+\mathrm{i}q_y}{\sqrt{2eB}}\right)^{l'-l}\mathrm{e}^{\mathrm{i}q_y\frac{q_x+2k_x}{2eB}}\mathrm{e}^{-\frac{\mathbf{q}^2}{4eB}}L_l^{l'-l}\left(\frac{\mathbf{q}^2}{2eB}\right). \qquad \text{(A.4)}
\end{aligned}$$

In the second to last line, I used formula 7.377. from [27], and in the last line, I used a property of the generalized Laguerre polynomials

$$\frac{(-x)^n}{n!}L_m^{n-m}(x)=\frac{(-x)^m}{m!}L_n^{m-n}(x). \qquad \text{(A.5)}$$

Appendix B

Derived quantum oscillation amplitudes

In the two-band model with interband impurity scattering and interactions, the amplitudes appearing in the thermodynamic potential Eq. (3.42) equal

$$A_\lambda^{(1)} = -\frac{(eB)^2}{4\pi^3 m_\lambda}; \tag{B.1}$$

$$A_\lambda^{(2)} = \frac{(eB)^2}{16\pi^3 m_\lambda}\left(1 - 2\pi\tilde{\alpha}_\lambda\tau_\lambda\right); \tag{B.2}$$

$$B_\lambda^{(2)} = -\frac{V_0\gamma_\lambda(eB)^2}{8\pi^4}; \tag{B.3}$$

$$A_+ = -\frac{\omega_+^2}{2\pi^2}\sum_\lambda \tilde{\beta}_\lambda m_\lambda\tau_\lambda; \tag{B.4}$$

$$B_+ = -\frac{V_0\delta(eB)^2}{4\pi^4}; \tag{B.5}$$

$$B_- = -\frac{V_0\delta(eB)^2}{4\pi^4}. \tag{B.6}$$

In the conductivities Eq. (3.45), the amplitudes differ in the longitudinal and transversal component. They turn out to be

$$C^{(1)}_{xx,\lambda} = \frac{W_{\bar{\lambda}}\beta_{\bar{\lambda}}\tau_{\bar{\lambda}}\left(4\tau_{\bar{\lambda}}^2-1\right)}{\omega_{\bar{\lambda}}\left(4\tau_{\bar{\lambda}}^2+1\right)^2} + \frac{W_\lambda\left(4\left(\alpha_\lambda-2\right)\tau_\lambda^3-\left(\alpha_\lambda+2\right)\tau_\lambda\right)}{\omega_{c\lambda}\left(4\tau_\lambda^2+1\right)^2}; \tag{B.7}$$

$$\begin{aligned} C^{(2)}_{xx,\lambda} &= \frac{W_{\bar{\lambda}}\left(\beta_\lambda\left(16\tau_{\bar{\lambda}}^4-1\right)\tau_{\bar{\lambda}}\left(2\pi\alpha_\lambda\tau_\lambda-1\right)+2\beta_{\bar{\lambda}}^2\left(4\tau_{\bar{\lambda}}^2-3\right)\tau_{\bar{\lambda}}^3\right)}{\omega_{c\bar{\lambda}}\left(4\tau_{\bar{\lambda}}^2+1\right)^3} \\ &+ \frac{2W_\lambda\tau_\lambda\left(\alpha_\lambda^2\left(4\tau_\lambda^2-3\right)\tau_\lambda^2-\alpha_\lambda\left(4\tau_\lambda^2+1\right)\left(\tau_\lambda\left(4\tau_\lambda\left(\pi\tau_\lambda+1\right)+3\pi\right)-1\right)\right)}{\omega_{c\lambda}\left(4\tau_\lambda^2+1\right)^3} \\ &+ \frac{2W_\lambda\tau_\lambda}{\omega_{c\lambda}\left(4\tau_\lambda^2+1\right)}; \end{aligned} \tag{B.8}$$

$$D^{(2)}_{xx,\lambda} = \frac{V_0\gamma_\lambda m_\lambda}{2\pi}\left(\frac{W_{\bar{\lambda}}\beta_{\bar{\lambda}}\tau_{\bar{\lambda}}\left(4\tau_{\bar{\lambda}}^2-1\right)}{\omega_{c\bar{\lambda}}\left(4\tau_{\bar{\lambda}}^2+1\right)^2} + \frac{W_\lambda(4\left(\alpha_\lambda-2\right)\tau_\lambda^3-\left(\alpha_\lambda+2\right)\tau_\lambda)}{\omega_{c\lambda}\left(4\tau_\lambda^2+1\right)^2}\right); \tag{B.9}$$

$$\begin{aligned} C_{xx,+} &= \sum_\lambda \frac{W_\lambda\beta_\lambda\tau_\lambda}{\omega_{c\lambda}\left(4\tau_\lambda^2+1\right)^3}\left(2\pi\left(16\tau_\lambda^4-1\right)\beta_{\bar{\lambda}}\tau_{\bar{\lambda}}+1\right. \\ &\left.+2\tau_\lambda\left(16\pi\left(\alpha_\lambda-2\right)\tau_\lambda^4+8\left(\alpha_\lambda-1\right)\tau_\lambda^3-6\alpha_\lambda\tau_\lambda-\pi\left(\alpha_\lambda+2\right)-16\pi\tau_\lambda^2\right)\right); \end{aligned} \tag{B.10}$$

$$D_{xx,+} = \sum_\lambda \frac{W_\lambda\delta V_0\tau_\lambda\left(\beta_\lambda\left(4\tau_\lambda^2-1\right)m_{\bar{\lambda}}+m_\lambda\left(4\left(\alpha_\lambda-2\right)\tau_\lambda^2-\alpha_\lambda-2\right)\right)}{2\pi\omega_{c\lambda}\left(4\tau_\lambda^2+1\right)^2}; \tag{B.11}$$

$$C_{xx,-} = \sum_\lambda \frac{W_\lambda\beta_\lambda\tau_\lambda\left(4\alpha_\lambda\left(4\tau_\lambda^2-3\right)\tau_\lambda^2-16\tau_\lambda^4+1\right)}{\omega_{c\lambda}\left(4\tau_\lambda^2+1\right)^3}; \tag{B.12}$$

$$D_{xx,-} = \sum_\lambda \frac{W_\lambda\delta V_0\tau_\lambda\left(\beta_\lambda\left(1-4\tau_\lambda^2\right)m_{\bar{\lambda}}+m_\lambda\left(-4\left(\alpha_\lambda-2\right)\tau_\lambda^2+\alpha_\lambda+2\right)\right)}{2\pi\omega_{c\lambda}\left(4\tau_\lambda^2+1\right)^2}; \tag{B.13}$$

$$C^{(1)}_{xy,\lambda} = -\frac{4W_{\bar{\lambda}}\beta_{\bar{\lambda}}\tau_{\bar{\lambda}}^2}{\omega_{c\bar{\lambda}}\left(4\tau_{\bar{\lambda}}^2+1\right)^2} + \frac{W_\lambda\left(-8\left(\alpha_\lambda-2\right)\tau_\lambda^2+16\tau_\lambda^4+3\right)}{2\omega_{c\lambda}\left(4\tau_\lambda^2+1\right)^2}; \tag{B.14}$$

$$\begin{aligned} C^{(2)}_{xy,\lambda} &= \frac{W_{\bar{\lambda}}\tau_{\bar{\lambda}}^2\left(\beta_{\bar{\lambda}}^2\left(1-12\tau_{\bar{\lambda}}^2\right)-4\beta_\lambda\left(4\tau_{\bar{\lambda}}^2+1\right)\left(2\pi\alpha_\lambda\tau_\lambda-1\right)\right)}{\omega_{c\bar{\lambda}}\left(4\tau_{\bar{\lambda}}^2+1\right)^3} \\ &+ \frac{W_\lambda\left(\alpha_\lambda^2\left(2\tau_\lambda^2-24\tau_\lambda^4\right)+2\alpha_\lambda\tau_\lambda\left(4\tau_\lambda^2+1\right)\left(8\tau_\lambda\left(2\pi\tau_\lambda^3+\pi\tau_\lambda+1\right)+3\pi\right)\right)}{2\omega_{c\lambda}\left(4\tau_\lambda^2+1\right)^3} \\ &- \frac{W_\lambda\left(4\tau_\lambda^2+3\right)}{2\omega_{c\lambda}\left(4\tau_\lambda^2+1\right)}; \end{aligned} \tag{B.15}$$

$$D^{(2)}_{xy,\lambda} = \frac{V_0 \gamma_\lambda m_\lambda}{4\pi} \left(-\frac{8\beta_{\bar{\lambda}} \tau_{\bar{\lambda}}^2}{\left(4\tau_{\bar{\lambda}}^2 + 1\right)^2} + \frac{2 - 8\left(\alpha_\lambda - 1\right)\tau_\lambda^2}{\left(4\tau_\lambda^2 + 1\right)^2} + 1 \right); \tag{B.16}$$

$$\begin{aligned} C_{xy,+} = \sum_\lambda \frac{W_\lambda \beta_\lambda \tau_\lambda}{\omega_{c\lambda}\left(4\tau_\lambda^2 + 1\right)^3} \big[& -8\pi \left(4\tau_\lambda^3 + \tau_\lambda\right) \beta_{\bar{\lambda}} \tau_{\bar{\lambda}} + 3\pi + 4\tau_\lambda \\ & + 2\tau_\lambda \alpha_\lambda \left(1 - 4\tau_\lambda \left(\tau_\lambda \left(4\pi\tau_\lambda + 3\right) + \pi\right)\right) \\ & + 4\tau_\lambda^2 \left(4\tau_\lambda \left(4\pi\tau_\lambda^3 + 5\pi\tau_\lambda + 1\right) + 7\pi\right) \big]; \end{aligned} \tag{B.17}$$

$$D_{xy,+} = \sum_\lambda \frac{W_\lambda \delta V_0 \left(m_\lambda \left(-8\left(\alpha_\lambda - 2\right)\tau_\lambda^2 + 16\tau_\lambda^4 + 3\right) - 8\beta_\lambda \tau_\lambda^2 m_{\bar{\lambda}}\right)}{4\pi\omega_{c\lambda}\left(4\tau_\lambda^2 + 1\right)^2}; \tag{B.18}$$

$$C_{xy,-} = \sum_\lambda \frac{2W_\lambda \beta_\lambda \tau_\lambda^2 \left(4\left(2 - 3\alpha_\lambda\right)\tau_\lambda^2 + \alpha_\lambda + 2\right)}{\omega_{c\lambda}\left(4\tau_\lambda^2 + 1\right)^3}; \tag{B.19}$$

$$D_{xy,-} = -\sum_\lambda \frac{W_\lambda \delta V_0 \left(m_\lambda \left(-8\left(\alpha_\lambda - 2\right)\tau_\lambda^2 + 16\tau_\lambda^4 + 3\right) - 8\beta_\lambda \tau_\lambda^2 m_{\bar{\lambda}}\right)}{4\pi\omega_{c\lambda}\left(4\tau_\lambda^2 + 1\right)^2}. \tag{B.20}$$

They were derived in *Mathematica* by expanding Eq. (3.43) with respect to the self-energy, combining products of trigonometric functions to obtain trigonometric functions of combinations, and then collecting terms with the same argument of the cosine.

Appendix C

Coulomb interactions and extended impurities

In this appendix, I discuss the possibility of extending my results to more generic forms of interactions and impurity potential. It will influence the oscillations through changing the form of the self energy.

C.1 Coulomb interactions

In two dimensions, the Fourier transform of the (unscreened) Coulomb interaction reads:

$$V(\mathbf{q}) = \frac{e^2}{|\mathbf{q}|}. \tag{C.1}$$

In this case, the Hartree diagram will be divergent, as it is proportional to V_0. As for the Fock contribution, I can plug $V_{\mathbf{q}}$ it into Eq. (3.19) and get

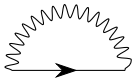

$$\begin{aligned}
&= -\frac{e^2\delta_{k_x,k'_x}\delta_{l,l'}}{2\pi\beta}\sum_{r,\omega_n}\int_0^\infty dq\,(-1)^{r-l}\mathrm{e}^{-\frac{q^2}{2eB}} \\
&\quad L_r^{l-r}\left(\frac{q^2}{2eB}\right)L_l^{r-l}\left(\frac{q^2}{2eB}\right)G_r^0(\mathrm{i}\omega_n) \\
&= -\frac{e^2\sqrt{eB}\delta_{k_x,k'_x}\delta_{l,l'}}{2\sqrt{2}\pi\beta}\sum_{r,\omega_n}\frac{(-1)^{r-l}\Gamma(\frac{1}{2})\Gamma(r+\frac{1}{2})}{r!\Gamma(r-l+\frac{1}{2})\Gamma(l-r+1)} \\
&\quad {}_3F_2\left(-r, l-r+\frac{1}{2}, \frac{1}{2}; -r+\frac{1}{2}, l-r+1; 1\right)G_r^0(\mathrm{i}\omega_n),
\end{aligned} \tag{C.2}$$

where ${}_3F_2$ is the hypergeometric function.This expression contains no divergences for any values of l, r. The hypergeometric function appearing here is

a finite sum:

$$ {}_3F_2\left(-r, l-r+\frac{1}{2}, \frac{1}{2}; -r+\frac{1}{2}, l-r+1; 1\right) = \sum_{n=0}^{r} \frac{(-r)_n (l-r+\frac{1}{2})_n (\frac{1}{2})_n}{(-r+\frac{1}{2})_n (l-r+1)_n n!}. \tag{C.3} $$

This form of the self-energy poses two problems for proceeding analytically. First of all, it is hard to evaluate the LL sum with the standard techniques described in 3.1. The reason is that after using the Poisson summation formula, extending the integration to the whole real line introduces additional poles. Second of all, to calculate the density of states or conductivity by the method of contour integration, one needs to solve the pole condition of the form

$$ \mathrm{i}\omega_n - \varepsilon_l - \Sigma_l(\mathrm{i}\omega_n) = 0, \tag{C.4} $$

which become difficult when the self-energy depends on l. However, the problem is tractable with numerical methods. In the sum over r in Eq. (C.2), terms with $r \approx l$ dominate, so only a few terms in the vicinity of l need to be summed. Then, evaluating the thermodynamic potential and conductivity with the obtained self energy is feasible.

C.2 Extended impurities

For impurity scattering, I consider a Gaussian scattering potential, which in Fourier space takes the form

$$ u_{\mathbf{q}} = u_0 e^{-\frac{\lambda^2 \mathbf{q}^2}{2}}, \tag{C.5} $$

with the impurity size λ. Plugging this into Eq. (3.15), the second-order contribution to the self energy reads

$$ \begin{aligned} &= \frac{n_{\mathrm{imp}} u_0^2 eB \delta_{k_x, k_x'} \delta_{l,l'}}{2\pi} \sum_r \int_0^\infty dq\, q (-1)^{r-l} \mathrm{e}^{-\frac{q^2}{2eB}(1+\kappa)} \\ &\quad L_r^{l-r}\left(\frac{q^2}{2eB}\right) L_l^{r-l}\left(\frac{q^2}{2eB}\right) G_r^0 \\ &= \frac{n_{\mathrm{imp}} u_0^2 eB \delta_{k_x, k_x'} \delta_{l,l'}}{2\pi} \sum_r \int_0^\infty dx\, \mathrm{e}^{-x(1+\kappa)} x^{r-l} \frac{l!}{r!} \left[L_l^{r-l}(x)\right]^2 G_r^0, \end{aligned} \tag{C.6} $$

where I defined $\kappa = 2eB\lambda^2$. At this point, an approximation can be made. Since only the high Landau levels $l \sim \frac{\mu}{\omega_c} \gg 1$ contribute to quantum oscillations, I can use that for large l

$$ L_l^r(x) \approx l^{\frac{r}{2}} e^{\frac{x}{2}} x^{-\frac{r}{2}} J_r(2\sqrt{lx}), \tag{C.7} $$

where J_r is the Bessel function of the first kind. Using this formula, the diagram simplifies to

$$
\begin{aligned}
&= \frac{N_{\text{imp}} u_0^2 eB}{2\pi} \sum_r \int_0^\infty dx e^{-\kappa x} \frac{l! l^{r-l}}{r!} \left[J_r \left(2\sqrt{lx} \right) \right]^2 G_r^0 \\
&= \frac{N_{\text{imp}} u_0^2 eB}{2\pi\kappa} e^{-\frac{2l}{\kappa}} l! \sum_r \frac{l^{r-l}}{r!} I_{r-l} \left(\frac{2l}{\kappa} \right) G_r^0 \\
&= \frac{N_{\text{imp}} u_0^2 eB}{4\pi^{\frac{3}{2}}\sqrt{\kappa}} l! \sum_r \frac{l^{r-l-\frac{1}{2}}}{r!} G_r^0,
\end{aligned}
\tag{C.8}
$$

where I_α is the Bessel function of the second kind and to obtain the last line I used its asymptotic expansion

$$
I_\alpha(z) \approx \frac{e^z}{\sqrt{2\pi z}} \tag{C.9}
$$

valid for $\alpha \ll z$. The expansion is justified, since only terms with $l \sim r$ contribute to the sum. The reason is that for $r < l$, the summed term is quickly damped by l^{r-l} (keeping in mind that l is large), and for large r, it is damped by $\frac{1}{r!}$. The expression can be further simplified by using the Stirling's approximation

$$
n! \sim \sqrt{2\pi n} \left(\frac{n}{\mathrm{e}} \right)^n \tag{C.10}
$$

valid for large n. Then

$$
= \frac{N_{\text{imp}} u_0^2 eB}{2\pi\sqrt{2\kappa}} \mathrm{e}^{-l} \sum_r \frac{l^r}{\Gamma(r+1)} G_r^0. \tag{C.11}
$$

The self-energy contribution for this kind of extended impurities turns out to be surprisingly simple. The Landau level summation could be evaluated using the standard techniques, as the summed term has only a single pole from the Green's function. The problem for proceeding analytically appears when computing the density of states and conductivity, as solving equation Eq. (C.4) is challenging.

Appendix D

Magnetic interaction

Magnetic interaction is an alternative mechanism producing similar predictions to the model proposed in this work. In this appendix, I compute the oscillations from magnetic interaction in the model considered in section 3.4 (based on a derivation in [22]).

The magnetic interaction mechanism consists of replacing the external magnetic field B with the mean magnetic field $B + \mu_0 M$ in formulas for the oscillating part of magnetization/conductivity (where $\mu_0 = 4\pi \times 10^{-7} \frac{\mathrm{H}}{\mathrm{m}}$ is the vacuum permeability constant). The justification for the replacement is that the magnetic field fluctuates on a much smaller scale than the magnetic length $l_B = \frac{1}{\sqrt{eB}}$. Since quantum oscillations arise from physics on the scale of the magnetic length, they must be governed by the mean magnetic field.

To obtain oscillations produced by magnetic interaction in the considered model, I need to insert the formula for M obtained from Eq. (3.42) into itself and into the formulas for conductivity oscillations in Eq. (3.43) and Eq. (3.44). Then, I expand in the Dingle factor R_D to get combination frequencies at second order. The term with the highest power of the large parameter $\frac{W_\lambda}{\omega_{c\lambda}}$ is the one produced by expanding the oscillating factor $\cos\left(2\pi \frac{F}{B+\mu_0 M}\right)$, the rest can be discarded.

Since I want to compare the predictions of the magnetic interaction model and the one developed in this thesis, I will focus on the difference frequency terms. Using the procedure described above, I get the following contributions

to magnetization and conductivities

$$M^- = -\frac{\mu_0 e^3}{4\pi^3}\sum_\lambda \frac{W_\lambda^2 W_{\bar\lambda}}{\omega_{c\lambda}^2 m_\lambda}\sin\left(2\pi\frac{W_-}{\omega_-}\right) \tag{D.1}$$

$$\times R_{LK}\left(\frac{2\pi^2 T}{\omega_{c1}}\right) R_{LK}\left(\frac{2\pi^2 T}{\omega_{c2}}\right) R_{D1}R_{D2}; \tag{D.2}$$

$$\sigma_{xx}^- = \frac{\mu_0\sigma_0^2}{2}\sum_\lambda \frac{W_\lambda^2 W_{\bar\lambda}\Gamma_\lambda}{\omega_{c\lambda}^2\omega_{c\bar\lambda}m_{\bar\lambda}(1+4\Gamma^2)}\cos\left(2\pi\frac{W_-}{\omega_-}\right) \tag{D.3}$$

$$\times R_{LK}\left(\frac{2\pi^2 T}{\omega_{c1}}\right) R_{LK}\left(\frac{2\pi^2 T}{\omega_{c2}}\right) R_{D1}R_{D2}; \tag{D.4}$$

$$\sigma_{xy}^- = -\frac{\mu_0\sigma_0^2}{8}\sum_\lambda \frac{W_\lambda^2 W_{\bar\lambda}(3+4\Gamma_\lambda^2)}{\omega_{c\lambda}^2\omega_{c\bar\lambda}m_{\bar\lambda}(1+4\Gamma^2)}\cos\left(2\pi\frac{W_-}{\omega_-}\right) \tag{D.5}$$

$$\times R_{LK}\left(\frac{2\pi^2 T}{\omega_{c1}}\right) R_{LK}\left(\frac{2\pi^2 T}{\omega_{c2}}\right) R_{D1}R_{D2}. \tag{D.6}$$

Apart from the form of the non-universal amplitudes, magnetic interaction produces the same contributions to observables as interactions between electrons. To distinguish between the two effects, another method than measuring the temperature dependence is needed. However as noted in [21], the effect from magnetic interaction is likely too small to explain the appearance of the difference frequency in magnetization measurements discussed in section 3.5.2.

Bibliography

[1] P. Drude. "Zur Elektronentheorie der Metalle". In: *Annalen der Physik* 306.3 (1900), pp. 566–613. DOI: https://doi.org/10.1002/andp.19003060312.

[2] E. Fermi. "Zur Quantelung des idealen einatomigen Gases". In: *Zeitschrift für Physik* 36 (1926), pp. 902–912. DOI: https://doi.org/10.1007/BF01400221.

[3] L. Landau. "The Theory of a Fermi Liquid". In: *Soviet Physics Journal of Experimental and Theoretical Physics* 3.6 (1957), p. 920.

[4] A.A. Abrikosov and I.M. Khalatnikov. "The theory of a fermi liquid (the properties of liquid 3He at low temperatures)". In: *Reports on Progress in Physics* 22.1 (1959). DOI: https://doi.org/10.1088/0034-4885/22/1/310.

[5] W. J. de Haas and P. M. van Alphen. "The dependence of the susceptibility of diamagnetic metals upon the field". In: *Proceedings of the Academy of Science of Amsterdam* 33 (1930), pp. 1106–1118.

[6] L. Shubnikov and W. J. de Haas. "Magnetic resistance increase in single crystals of bismuth at low temperatures". In: *Proceedings of the Royal Netherlands Academy of Arts and Science* 33 (1930), pp. 130–133.

[7] L. Onsager. "Interpretation of the de Haas-van Alphen effect". In: *The London, Edinburgh, and Dublin Philosophical Magazine and Journal of Science* 43.344 (1952), pp. 1006–1008.

[8] I.M. Lifshitz and A.M. Kosevich. "Theory of magnetic susceptibility in metals at low temperatures". In: *Sov. Phys. JETP* 2.4 (1956), pp. 636–645.

[9] Nico Huber et al. "Quantum Oscillations of the Quasiparticle Lifetime in a Metal". In: *Nature* 621 (2023), pp. 276–281. DOI: 10.1038/s41586-023-06330-y.

[10] B.S. Tan et al. "Unconventional Fermi surface in an insulating state". In: *Science* 349.6245 (2015). DOI: https://doi.org/10.1126/science.aaa7974.

[11] Z. Xiang et al. "Quantum oscillations of electrical resistivity in an insulator". In: *Science* 362.6410 (2018). DOI: https://doi.org/10.1126/science.aap9607.

[12] Zhongdong Han et al. "Anomalous Conductance Oscillations in the Hybridization Gap of InAs/GaSb Quantum Wells". In: *Phys. Rev. Lett.* 123 (12 2019), p. 126803. DOI: 10.1103/PhysRevLett.123.126803.

[13] V. Leeb et al. "Anomalous Quantum Oscillations in a Heterostructure of Graphene on a Proximate Quantum Spin Liquid". In: *Phys. Rev. Lett.* 126 (9 2021), p. 097201. DOI: 10.1103/PhysRevLett.126.097201.

[14] T. Terashima et al. "Heavy fermions survive the metamagnetic transition in UPd_2Al_3". In: *Phys. Rev. B* 55 (20 May 1997), R13369–R13372. DOI: 10.1103/PhysRevB.55.R13369.

[15] Clifford W. Hicks et al. "Quantum Oscillations and High Carrier Mobility in the Delafossite $PdCoO_2$". In: *Phys. Rev. Lett.* 109 (11 Sept. 2012), p. 116401. DOI: 10.1103/PhysRevLett.109.116401.

[16] F. Arnold et al. "Fermi surface of $PtCoO_2$ from quantum oscillations and electronic structure calculations". In: *Phys. Rev. B* 101 (19 May 2020), p. 195101. DOI: 10.1103/PhysRevB.101.195101.

[17] Zheng Chen et al. "Three-dimensional topological semimetal phase in layered $TaNiTe_5$ probed by quantum oscillations". In: *Phys. Rev. B* 103 (3 2021), p. 035105. DOI: 10.1103/PhysRevB.103.035105.

[18] V. Leeb and J. Knolle. "Theory of difference-frequency quantum oscillations". In: *Phys. Rev. B* 108 (5 Aug. 2023), p. 054202. DOI: 10.1103/PhysRevB.108.054202.

[19] S. Engelsberg and G. Simpson. "Influence of Electron-Phonon Interactions on the de Haas-van Alphen Effect". In: *Phys. Rev. B* 2 (6 1970), pp. 1657–1665. DOI: 10.1103/PhysRevB.2.1657.

[20] A Wasserman and M Springford. "The influence of many-body interactions on the de Haas-van Alphen effect". English. In: *Advances in Physics* 45 (1996), pp. 471–503. ISSN: 1460-6976.

[21] Andrew A. Allocca and Nigel R. Cooper. "Low-frequency quantum oscillations from interactions in layered metals". In: *Phys. Rev. Res.* 3 (4 2021), p. L042009. DOI: 10.1103/PhysRevResearch.3.L042009.

[22] D. Shoenberg. *Magnetic Oscillations in Metals*. Cambridge University Press, 1984.

[23] L. Landau. "Diamagnetismus der Metalle". In: *Zeitschrift für Physik* 64 (1930), pp. 629–637.

[24] Antoine J.F. Bastin et al. "Quantum oscillations of the hall effect of a fermion gas with random impurity scattering". In: *Journal of Physics and Chemistry of Solids* 32 (1971), pp. 1811–1824.

[25] L. Smrčka and L. Streda. "Transport coefficients in strong magnetic fields". In: *Journal of Physics C: Solid State Physics* 10.12 (1977).

[26] P. Streda. "Theory of quantised Hall conductivity in two dimensions". In: *Journal of Physics C: Solid State Physics* 15.22 (Aug. 1982), p. L717. DOI: 10.1088/0022-3719/15/22/005.

[27] I.S. Gradshteyn and I.M. Ryzhik. *Table of Integrals, Series, and Products (Eighth Edition)*. Academic Press, 2014.

Statement of authorship

I hereby declare that the thesis submitted is my own unaided work. All direct or indirect sources used are acknowledged as references.

I am aware that the thesis in digital form can be examined for the use of unauthorized aid and in order to determine whether the thesis as a whole or parts incorporated in it may be deemed as plagiarism. For the comparison of my work with existing sources I agree that it shall be entered in a database where it shall also remain after examination, to enable comparison with future theses submitted. Further rights of reproduction and usage, however, are not granted here.

This paper was not previously presented to another examination board and has not been published.